Model-assisted estimation of change in forest biomass over an 11 year period in a sample survey supported by airborne LiDAR: A case study with post-stratification to provide "activity data"

Authors:

Erik Næsset[a,*], Ole Martin Bollandsås[a], Terje Gobakken[a], Timothy G. Gregoire[b], Göran Ståhl[c]

[a] Department of Ecology and Natural Resource Management, Norwegian University of Life Sciences, P.O. Box 5003, NO-1432 Ås, Norway

[b] School of Forestry and Environmental Studies, Yale University, 360 Prospect Street, New Haven, CT 06511-2189, USA

[c] Department of Forest Resource Management, Swedish University of Agricultural Sciences, SE-90183 Umeå, Sweden

*Corresponding author:

Erik Næsset

E-mail address: erik.naesset@umb.no

Phone: +47 64965734

Fax: +47 64965802

Abstract

The United Nations Collaborative Program on Reduced Emissions from Deforestation and Forest Degradation in Developing Countries (UN REDD) was launched with the aim of contributing to the development of capacity for reducing emissions from loss of forest carbon in developing countries. It is understood that REDD mechanisms must be supported by forest assessment programs that can monitor the carbon stocks by carbon pools and human activities. Reporting at a national level will be required but many countries are likely to benefit from more local monitoring programs within the countries as well, gauging the effects of national policies and local financial mechanisms aimed at reaching goals for emission control for the nation as a whole. Field-based forest sample surveys are typically used as support for national reporting purposes. However, monitoring within the countries will require huge investments in field surveys to provide reliable change estimates with high spatial and temporal resolution. Airborne scanning LiDAR has emerged as a promising tool to provide auxiliary data for sample surveys aiming at estimation of above-ground tree biomass. The aim of this study was to demonstrate how "wall-to-wall" LiDAR data can be used for change estimation. Estimators for areal changes of categories representing human activities such as "deforestation", "degradation" and "untouched" were presented. Corresponding estimators for variance were also provided. Furthermore, it was shown how net change in biomass for the defined activity categories and for the entire area of interest can be estimated from a field sample survey with and without support of LiDAR remote sensing data and how the uncertainty can be quantified by corresponding variance estimates. In a case study in a small boreal forest area in southeastern Norway (852.6 ha) a probability sample of 176 field sample plots distributed according to a stratified systematic design was measured twice over an 11 year period. Corresponding multi-temporal scanning LiDAR data were also available. A multinomial logistic regression model was used to predict change category for every LiDAR grid cell in the area, and areal changes were estimated from the pure field sample and with the support of the LiDAR data applying model-assisted estimators. The standard errors of the areal change estimates were reduced by 43-75% by adding LiDAR data to the estimation. The change categories were used as post-strata in a subsequent estimation of net change in biomass. The standard errors of the biomass change estimates for the respective change categories were reduced by 18-84% compared to the pure field survey when using LiDAR data as auxiliary information in a model-assisted estimation procedure, which translates to a need for 1.5-38.7 times as many field plots when relying only on the field data. For the entire area of interest, the standard error of the overall net change in biomass was reduced by 57% compared to the uncertainty reported from the pure field survey.

1. Introduction

Reliable estimation of changes in different forest carbon pools has for several reasons become a prominent issue in forest inventory at a broad range of geographical scales.

Countries ratifying the Kyoto Protocol to the United Nations Framework Convention on Climate Change are committed to report their direct human induced emissions and removals of carbon dioxide in the commitment period 2008–2012, including emissions and removals in the land use and forestry sectors (UNFCCC, 2008). Field-based nation-wide sample surveys, such as the national forest inventory programs in Europe or the Forest Inventory and Analysis (FIA) program of the U.S. Forest Service in the U.S.A. are typically used for such reporting purposes (Rypdal et al., 2005; Woodbury et al., 2007).

The United Nations Collaborative Program on Reduced Emissions from Deforestation and Forest Degradation in Developing Countries (UN REDD) (http://www.un-redd.org) was launched with the aim of contributing to the development of capacity for reducing emissions from loss of forest carbon in developing countries. It is understood that REDD mechanisms must be supported by forest assessment programs that can monitor the carbon stocks. Reporting at national level will be required [see example from Guyana (Anon., 2009)] but many countries are likely to benefit from more local monitoring programs within the countries as well, gauging the effects of national policies and local financial mechanisms aimed at reaching goals for emission control for the nation as a whole. In Tanzania for example, it is recognized that the REDD initiative will provide incentives for local communities participating in forest management (Anon., 2010). Accessing carbon finances through REDD requires, among other things, measurement of carbon stock changes in forests (Anon., 2010). Some demonstrations of local monitoring and engagement of local villagers in so-called “participatory inventory” and “participatory forest carbon assessment” are currently taking place in countries like Tanzania (Mukama et al., 2012).

Any future mechanism for commercial trading of forest carbon credits earned through active forest management to increase carbon sequestration will also require trustworthy systems for measurement, reporting, and verification of carbon offset activities. Such systems will most likely have to be adopted locally since they must be capable of capturing changes in carbon stocks at the geographical level at which contracts are established (e.g. individual forest estates).

Most forest inventories implemented as sample surveys at national level are designed to serve multiple purposes (Tomppo et al., 2010). They typically provide information on a wide array of variables characterizing the current timber stock and the environmental conditions in broad terms, as well as changes in such parameters over time through repeated measurements. Thus, such national surveys are often simple and robust in their designs. Systematic designs are commonly adopted and it is often preferred to avoid stratified sampling except for stratification into broader geographical regions allowing more intense sampling in certain areas. Although stratification can be efficient with respect to estimation of one or a few variables at a given point in time, the same stratification may be inefficient with respect to other variables or future observations as the structure of the forest changes over time. With a simple and unstratified design estimates for any sub-set of the population may easily be obtained for any variable and at any point in time, provided availability of samples in the sub-set in question.

At local levels, however, there does not seem to be a commonly adopted practice in designing forest inventories. In developed countries, forest management inventories conducted for individual forest estates or for numerous estates within a municipality, district, or region are in many cases – like in the Nordic countries – the most reliable source of information on local forest resources and carbon stocks. Such inventories are often designed to provide estimates of current timber resources as cost-efficiently as possible and they are less focused on being simple and robust in their designs to allow flexibility for future monitoring of changes. Thus, a potential need for future assessment of the resources and estimates of changes over time is usually not reflected in the design. Whenever a sample survey is part of the overall inventory, a stratification deemed efficient for estimation of current timber resources is often employed (e.g. Næsset, 2002, 2004). Examples of stratification criteria of relevance to boreal forests in particular are tree species, forest stand age or stage of development, and site productivity (e.g. Næsset, 2002).

The methodology employed in such local or district-wise inventories may be considered an option for measurement and verification of carbon offset activities or local monitoring of carbon stocks under REDD (Næsset et al., 2011). Identifying the specific management activities leading to enhanced carbon stocks will most likely be needed under a carbon offset mechanism. Changes in carbon stocks may be reported for various activities, such as deforestation and forest degradation under REDD as well. If such estimates are to be inferred from a sample survey, areas of deforestation, forest degradation, or other relevant activities must be identified. In a REDD context, satellite remote sensing with multi-temporal acquisitions has been proposed for identifying areas subject to such human activities. Further, in order to provide separate estimates of changes in carbon stocks for areas subject to for example degradation and deforestation the sample may be divided into classes deemed relevant for reporting. Such classes may be considered as post-strata in the estimation. A previous (pre-) stratification of the area in question may complicate the estimation based on a post-stratification if the post-strata cut across the initial strata and the initial stratification has adopted unequal sampling intensities, and/or the resulting post-strata have few or no samples for one or more of the initial strata while these combinations of post-strata and pre-strata are present in the population.

Various remote sensing techniques are commonly adopted for estimation of forest resources and are considered essential for REDD monitoring, although uncertainties are not always quantified and they may even be large if proper field data are not used as part of the applied estimation procedure. Nevertheless, classification and stratification of the forest and of different types of human activities are essential tasks in which remote sensing may assist. Remote sensing data treated as auxiliary to field data may also be useful for estimation of e.g. forest area or biomass. Techniques that use remotely sensed data may improve precision of the estimates significantly. Estimation with support of remote sensing data relies on extensive use of models. These models relate the remote sensing observables, like digital numbers in an image acquired by an imaging sensor, to a variable of interest measured on the ground, like forest/non-forest or biomass. Recent examples are (1) estimates of forest area for a part of Minnesota, U.S.A., provided by a sample of field plots from the FIA program supported by Landsat data through a logistic regression model for predicting proportion forest (McRoberts, 2010), (2) estimates of above-ground biomass provided for a district in Norway by a local field sample survey supported by airborne LiDAR data through a nonlinear regression model predicting biomass (Næsset et al., 2011), and (3) use of national forest inventory sample plots and LiDAR data to post-stratify by means of logistic regression model predictions to provide estimates of proportion forest area and growing stock volume for a region in Norway (McRoberts et al., 2012a).

Airborne LiDAR has emerged as one of the most promising remote sensing technologies for estimating above-ground tree biomass and thus carbon stored in trees. LiDAR depicts the horizontal and vertical distribution of biological material with high spatial resolution, and this information can be used for estimation of biomass. In several countries, airborne scanning LiDAR has during the last decade been used operationally for forest management inventories at a typical district level (~50-2000 km^2) (Næsset, 2004). Although operational use of airborne LiDAR for forest resource assessment seems to be most common in boreal and temperate forests (McRoberts et al., 2010), promising results for estimating biomass of tropical forests have also been reported (Nelson, 1997; Nelson et al., 1997; Weishampel et al., 2000; Drake et al., 2002, 2003; Lefsky et al., 2002; Clark et al., 2004; Asner et al., 2010). Studies of change estimation with LiDAR are still few though, but there is increasing evidence of the potential of the technology even for change estimation. Recent studies have focused on estimation of height increment of single trees (St-Onge & Vepakomma, 2004; Yu et al., 2004, 2005, 2006) and mean height (Næsset & Gobakken, 2005; Hopkinson et al., 2008; Yu et al., 2008), or volume growth (Næsset & Gobakken, 2005; Yu et al., 2008) and growth of stand basal area (Næsset & Gobakken, 2005).

A particular challenge is related to modeling of change observations by which the response variable can attain positive as well as negative values because it may restrict the choice of model form. Change in biomass is one such variable. Biomass in forests can typically increase over time by for example reforestation and growth in existing forests, while deforestation, forest degradation, natural mortality, and various types of management in forest remaining forest, such as final fellings, commercial thinning, and other harvest operations will result in a negative response (loss of biomass). Bollandsås et al. (2012) addressed various approaches to modeling of positive and negative changes in biomass using LiDAR-derived metrics as explanatory variables. In estimation of changes in biomass over a landscape with support of auxiliary data from LiDAR, one may either consider a joint modeling of negative and positive responses by various techniques or one may choose a strategy by which areas subject to loss of biomass are identified and separated from those subject to increase in biomass. The various processes (gain and loss of biomass) may then be modeled separately. The latter strategy is appealing in e.g. a REDD context provided that the different areas can be identified and classified prior to estimation, since it coincides well with the need to report on changes in carbon stocks according to activities (e.g. degradation and deforestation). LiDAR data may even assist in the required classification. Estimates of areas associated with different activities may be obtained by support of a LiDAR-based classification.

When LiDAR is used for estimation of timber resources and biomass and changes in these parameters over time, field plots co-registered with the remotely sensed data must be measured in order to develop predictive models for these parameters. In forest management inventories the field sample surveys are sometimes conducted according to systematic designs with a random start (Næsset, 2007) or according to random designs and frequently also stratified on the basis of prior information about the forest (Næsset, 2004). Because of the randomization in the selection of population elements for the field sample, design-based approaches to estimation and inference may be applied and one may take advantage of the rich suite of available design-unbiased or approximately design-unbiased estimators found in the literature. In a recent study, Næsset et al. (2011) demonstrated how biomass for an area of interest (AOI) could be estimated from a stratified probability sample of ground plots supported by wall-to-wall auxiliary data from LiDAR applying a model-assisted generalized regression estimator (Särndal et al., 1992). Model-assisted estimators use predictions of a fairly large sample of population elements (or even all population elements as in the current study) obtained from auxiliary data (e.g. LiDAR) to enhance the precision but rely on observations (e.g. field sample plots) for population elements selected from a probability sample for validity (McRoberts, 2010). Other studies on estimation of forest properties taking a design-based approach with LiDAR as auxiliary data include studies where the LiDAR data themselves constitute a sample in a two-phase or two-stage design (Parker & Evans, 2004; Andersen et al., 2009; Gregoire et al., 2011; Gobakken et al., 2012; Ene et al., 2012; McRoberts et al., 2012a,b; Nelson et al., 2012; Stephens et al., 2012) as well as studies where the LiDAR data cover the entire population (Andersen & Breidenbach, 2007; Corona & Fattorini, 2008; Pesonen et al., 2010). Recent studies have also demonstrated how different areal categories within an AOI can be estimated in a model-assisted way using remote sensing data as auxiliary information (McRoberts, 2010, 2011; McRoberts et al., 2012a).

In the present study, the overall objective was to demonstrate how areal changes for different categories of management activities and associated changes in biomass can be estimated for an AOI by repeated measurements of a stratified probability sample of field plots supported by coincident and repeated measurements with airborne scanning LiDAR. Specifically we compared areal estimates and associated estimates of change in biomass using a direct estimation approach (i.e., based purely on the field sample) and a model-assisted approach with LiDAR data as auxiliary information. The model-assisted strategy took advantage of three alternative approaches to predicting change in biomass over time. Corresponding variance estimates were also provided and compared in order to demonstrate what one potentially may gain in terms of reduced uncertainties by adding LiDAR data to the field survey. This study covered changes over a time span of 11 years (1999-2010).

2. Material and methods

2.1. Study area

This study was conducted in a boreal forest area in Våler Municipality (59°30′N, 10°55′E, 70–120 m a.s.l.) located in south-eastern Norway. The total area was 852.6 ha. The dominant tree species are Norway spruce (*Picea abies* (L.) Karst.) and Scots pine (*Pinus sylvestris* L.). Younger stands tend to have a larger portion of deciduous species than mature stands. Birch (*Betula pubescens* Ehrh.) is the dominant deciduous species. Further details about the study area can be found in Næsset (2002).

The forest in the area is actively managed for timber production according to standard silvicultural practices typically seen in boreal forests. Stands are usually harvested by clear-felling on the most productive sites while selective logging, such as shelterwood cutting, is more common on poor sites. Planting is a common regeneration method after clear-felling while selective logging often is followed by natural regeneration, especially in pine-dominated stands. Commercial thinning is also a frequent treatment.

The study took advantage of an existing operational stand-based forest inventory conducted in 1996. The aim of the operational inventory was to provide data for forest planning. We collected observations for a probability sample of field plots in a sample survey carried out in 1998 and 1999. Airborne scanning LiDAR data were acquired in 1999. In 2010, all sample plots were re-measured and a second airborne scanning LiDAR campaign was conducted.

2.2. Initial classification of the area – as per 1999

Aerial stereo photography was interpreted to delineate and classify forest stands according to the criteria age class, site productivity, and tree species. The aerial photographs (Agfa Aviphot Pan 200 PE1 panchromatic black-and-white film) were acquired 13 May 1996 and stand boundaries were recorded by photo-interpretation using a Wild B8 stereo-plotter equipped with linear encoders. The photo-interpretation was used as prior information in designing the inventory. At the time of designing the sample survey (March 1998), we used the stand map from 1996 as basis for the classification and allocation of sample plots to the various classes, see details below. The map was updated in 1999 by means of the 1999 LiDAR data for all clear-fellings that had taken place between 1996 and 1999. Thus, the final map was up to date as per the time of the LiDAR acquisition in 1999. The target population of the current study did not include areas that had been recently clear-felled (stands younger than 20 yrs, see below). Since recently regenerated forests stands (forest class I, see below) were the only stands where field plots were measured in 1998 while all young and mature stands were measured in 1999, any clear-felling in the period between 1998 and 1999 did not affect our field measurements and target population as defined per the time of the LiDAR acquisition in 1999. The population as defined in 1999 was therefore fully consistent with the sample survey as per 1999 and the sample was a pure probability sample. The following four forest classes were defined *a priori*:

Forest class I: Recently regenerated forest (age ≥20 yrs).
Forest class II: Young forest.
Forest class III: Mature forest. Spruce dominated.
Forest class IV: Mature forest. Pine dominated.

The areas of these four classes in the 852.6 ha study region were 65.8, 120.9, 140.4, and 195.6 ha, respectively, i.e., a total of 522.7 ha. These four classes constitute our AOI (Fig. 1). The average stand size was 1.4 ha. The remaining part of the study region not included in the defined population was mainly agricultural areas and recently clear-felled forest areas.

[FIGURE 1]

2.3. Sampling design

The field sample plot survey covering the four aforementioned forest classes was conducted in 1998 and 1999. The total budget allowed for approximately 175 plots to be measured (the final sample contained 176 plots, see Table 1). A systematic stratified design was employed. We aimed for approximately equal numbers of plots for the four classes. However, one of the classes (forest class IV) would get too many plots by pure proportional allocation, given the anticipated variation within this class based on experience from other, but similar forests. The sampling fraction in class IV was therefore reduced to 1/3 of the other classes. At the time of planning the survey digital maps were not available, and the systematic sampling plan was designed by creating squared and rectangular grids on a paper copy of the forest class map (Fig. 1). We determined to let a common grid be applied to classes I-III and a separate grid to class IV. Thus, two grids that had a random start were used and they had a plot distance of 150×150 m in forest classes I-III and 150×450 m in class IV. The final plot numbers and the geographical distribution of the plots are shown in Table 1 and Fig. 1, respectively. Because forest classes I-III shared the same systematic sampling plan, they were treated as a single stratum in the estimations. Thus, all the estimations in the current study were based on two pre-defined strata denoted as “pre-strata”. Forest classes I-III constituted “pre-stratum 1” whereas forest class IV was treated as a separate stratum and denoted as “pre-stratum 2”.

2.4. Field sample survey

2.4.1. The survey of 1998 and 1999

Topographic maps of the official Economic Map Series in scale 1:5000 were used to locate each plot in the field according to the predefined positions. When the plot centers were determined, they were marked with a wooden stick.

The 31 plots in forest class I (belonging to pre-stratum 1) were measured during summer and fall 1998 (Næsset & Bjerknes, 2001). However, when the field protocol for the measurements on these plots was designed in 1998, the main objective was collection of tree heights for studies of relationships between airborne LiDAR height measurements and tree heights. Thus, the only measurements made were tree heights on sample trees selected for estimation of dominant height on each plot [see further details in Næsset & Bjerknes (2001)]. Since biomass estimation was at that time not a concern, we did not record essential variables for quantifying biomass, such as for example stem number. For the current study, we considered that biomass estimation based only on tree heights would introduce large uncertainties due to the large likely variability in stem numbers. For example, in a dataset from a similar forest and age class Næsset (2011) reported a range in stem number between plots of 500-20500 trees ha^{-1}. Thus, our best judgment suggested that biomass estimation based on the 2010 measurements (see below) with a subsequent growth adjustment would be the least error-prone method for estimation of biomass in 1999. Therefore, the above-ground biomass estimates of 2010 (AGB_{2010}, see below) were adjusted by growth predictions. The species-specific stand volume growth models by Blingsmo (1988) were used to predict the foregone volume growth based on stand volume, stand age, and site index as independent variables. We assumed the same growth rates for biomass as for stand volume. Hence, biomass for the plots in forest class I in 1999 was predicted by adjusting AGB_{2010} by the ratio between the plot-wise estimates of stand volume in 2010 and 1999. In the following we will denote this predicted plot-level biomass as ”observed total above-ground biomass” (AGB_{1999}) even though the predicted values most likely will be subject to significant errors. A summary of these field-predicted data is presented in Table 1.

Differential Global Positioning System (GPS) and Global Navigation Satellite System (GLONASS) were used to determine the position of the center of each field plot. Two Javad Legacy 20-channel dual-frequency receivers observing pseudorange and carrier phase of both GPS and GLONASS were used as base- and rover receivers, respectively. The mean distance between the plots and the base station was approximately 19 km, and the rover receiver recorded data with a logging rate of 2 s for approximately 15 min on each plot. The antenna height of the rover receiver was approximately 4 m. The accuracy of the computed coordinates was expected to be better than 0.5 m (Næsset & Bjerknes, 2001).

[TABLE 1]

The 55, 58, and 32 plots in forest classes II (belonging to pre-stratum 1), III (belonging to pre-stratum 1), and IV (constituting pre-stratum 2), respectively, were measured during summer 1999 (Næsset, 2002). The plots were circular with an area of 200 m^2. On each of these 145 plots, all trees with diameter at breast height (d_{bh}) ≥4 cm were callipered. On 81 of the plots, all tree heights were measured. On the remaining 64 plots, tree heights were measured on sample trees selected with equal probability. The number of trees with height measurements ranged from 3 to 43 per plot with an average of 17.8. The heights were measured with a Vertex hypsometer.

Biomass was estimated as the sum of the individual components stump, stem, bark, dead and living branches, and foliage of individual trees predicted using previously fitted species-specific allometric models with single tree d_{bh} and tree height as independent variables (Marklund, 1988) following the procedure outlined in Næsset & Gobakken (2008). The estimated biomass for each plot was scaled to obtain AGB_{1999} (Mg ha^{-1}).

Differential GPS+GLONASS were used to determine the position of the center of each field plot following the procedure described above. However, collection of data lasted somewhat longer (15-30 min) than for forest class I. The antenna height was approximately 3.6 m for all points. The accuracy of the computed coordinates was expected to range from <0.1 m to 2.5 m with an average of approximately 0.3 m (Næsset, 2002).

2.4.2. The survey of 2010

Each of the 176 sample plots was revisited during summer and fall in 2010 and early spring 2011. With the coordinates registered in 1998/1999 as targets, a Topcon Legacy-E+ 40 channel dual-frequency receiver was used in real-time kinematic mode to navigate to each sample plot. For many of the sample plots the wooden stick used to mark the center in 1998/1999 was recovered and the center position was thus confirmed. However, for those sample plots where the stick could not be found, new GPS+GLONASS recordings were carried out following the same procedure as in 1998/1999. The recordings were conducted for the point where the real-time kinematic positions indicated the sample plot centre to be. Back in the office, the recorded GPS+GLONASS data were post-processed with correction data from the base station. Then angle and distance between post-processed coordinates of 2010 and 1998/1999 were calculated and the sample plot center was re-established by means of a compass and tape measure.

When the sample plot center had been identified, the stage of stand development was determined to correspond to the classification used for the forest classes in 1998. Twenty-four of the sample plots were classified as recently regenerated (corresponding to class I). Because it can be very laborious and expensive to measure small and recently regenerated trees (height >0.1 m), only a sample of sub-plots within the 200 m^2 sample plot were measured for these 24 plots. The sample plots in this particular class therefore consisted of four sub-plots with centers located 5.1 m from the sample plot center in each of the cardinal directions. Each sub-plot with an area of 20 m^2 was divided into four quadrants. On each sub-plot, d_{bh} of each tree taller than breast height (tally trees) was measured. For all remaining trees with heights between 0.1 m and breast height, d_{bh} was set to zero. Sample trees for height measurements were selected systematically as the first tree in each quadrant going clockwise around the sub-plots. Thus, potentially four trees per sub-plot and 16 trees per sample plot were selected.

Biomass models (Marklund, 1988) dependent on height and diameter were applied to predict biomass by components for each tree on the 20 m^2 sub-plots. First, species specific diameter-height models were fitted from the sample trees ≥1.3 m in height. These models were of the form $\hat{h} = 1.3 + \alpha d_{\mathrm{bh}}^{\beta}$. Height predictions for tally trees with d_{bh} >0 were then obtained. Then biomass was predicted using the models of Marklund (1988). For tally trees with d_{bh}=0, height was set as the species-specific average height of the sample trees with height <1.3 m. Biomass was estimated by scaling the biomass of a tree with height equal to 1.3 m and d_{bh}=0 with the ratio between average height and 1.3 m. Finally, single-tree biomass estimates were summed for each plot and scaled with the sampled area to obtain a per hectare value (AGB_{2010}).

In 2010, there were 41, 74, and 37 sample plots in classes corresponding to the definitions of forest classes II, III, and IV, respectively. The plot area for these classes in the 2010 survey was 400 m^2, but only data for an inner circle of 200 m^2 was used in the current study so that the plot size would correspond to that of the 1999 survey. All trees with d_{bh} ≥4 cm were measured for d_{bh}, species, and polar coordinates relative to the plot center. Heights were measured for sample trees selected with a probability proportional to stem basal area. The biomass calculation was similar to that of the 1999 survey, see above. The plot level biomass estimates were denoted AGB_{2010} (Mg ha^{-1}).

Finally, we estimated the change in total above-ground biomass (δAGB) for each individual plot as the difference between the plot-wise AGB_{2010} and AGB_{1999} values. Thus, δAGB (Mg ha^{-1}) is considered our observed change in total above-ground biomass in the subsequent analysis.

2.5. Airborne scanning LiDAR data

2.5.1. The 1999 LiDAR campaign

Airborne LiDAR data were acquired under leaf-on conditions on 8-9 June 1999 (Table 2). LiDAR data were collected with an Optech ALTM 1210 laser scanner carried by a fixed-wing aircraft flying at an altitude of approximately 700 m a.g.l. The pulse repetition frequency was 10 kHz and the scan frequency was 21 Hz, resulting in a point density on the ground of approximately 1.2 m^{-2}.

A complete postprocessing of the first and last echo data was undertaken by the contractor (Fotonor, Norway) by means of proprietary software provided by Optech Inc., Canada. All ranges measured by the laser at an off nadir angle, i.e., distances to the ground as well as to the tree canopy, were converted to vertical distances.

Unlike current state-of-the-art laser scanners (as per 2012), the old ALTM 1210 sensor has two electronic circuits recording the first and last echoes separately. After postprocessing, a few long last return ranges that exceeded the distance to the ground by up to 50 m were present in the data. According to the manufacturer these erroneous ranges were caused by a faulty last return sensor. A second flight was therefore carried out on 6 June 2000 to collect last return data with the only purpose of constructing the terrain model. Flying height corresponded to that of the first flight in 1999.

The ranging device had been calibrated by Optech Inc. and the operating firm always calibrated the system after installation in the aircraft. In addition, we established 30 circular control plots on plane road segments distributed throughout the study area for range calibration. Their positions were determined by differential GPS+GLONASS based on accurate dual-frequency carrier phase observations. Based on this calibration, the computed ranges of the first echo data acquired in 1999 were reduced by 0.13 m. The last echo ranges collected in 1999 and 2000 were extended by 0.46 m and reduced by 0.11 m, respectively.

The last echo data collected in 2000 were only used to extract the ground surface. This processing was conducted by the contractor. Ground echoes were classified by means of a filtering algorithm discarding local maxima assumed to represent vegetation hits using Optech's proprietary software, see further details in Næsset (2002). A triangulated irregular network (TIN) was generated from the planimetric coordinates of the classified terrain points. The 1999 first and last echo data (except for those pulses with erroneous ranges) were georeferenced to the year 2000 TIN surface, and heights above the TIN surface were calculated for all echoes by subtracting the respective TIN heights from the height values of the recorded echoes. The first and last echoes with corresponding relative height values were denoted as "first" and "last" echoes, respectively, and stored for subsequent analysis.

2.5.2. The 2010 LiDAR campaign

In the 2010 campaign, the LiDAR data were acquired under leaf-on conditions on 2 July (Table 2). The data were collected with an Optech ALTM Gemini laser scanner operated at an altitude of approximately 900 m a.g.l. The pulse repetition frequency was 100 kHz and the scan frequency was 55 Hz. The point density on the ground was approximately 7.3 m^{-2}. Previous research has shown that accuracy of biophysical plot and stand properties (e.g. basal area, mean tree height, and timber volume) estimated from airborne LiDAR data is fairly stable for point densities >0.1 m^{-2} (Holmgren, 2004; Maltamo et al., 2006; Gobakken & Næsset, 2008). Although the 2010 LiDAR data were collected primarily for other research purposes (studies of single-trees) and the point density thus may seem higher than needed for the current study, we believe they were relevant for change estimation with the 1999 LiDAR data as reference.

The 2010 LiDAR data were initially processed by the contractor (Blom Geomatics, Norway). Planimetric coordinates and ellipsoidal height values were computed for all echoes. Ground echoes were found and classified using the progressive TIN densification algorithm (Axelsson, 2000) of the TerraScan software (Anon., 2005). A TIN model was created from the planimetric coordinates and corresponding heights of the LiDAR echoes classified as ground points. The heights above the ground surface were calculated for all echoes by subtracting the respective TIN heights from the height values of all echoes recorded.

The ALTM Gemini sensor is capable of recording up to four echoes per pulse. In this study, we used the three echo categories classified as “single”, “first of many”, and “last of many”. The “single” and “first of many” echoes were pooled into one dataset denoted as “first” echoes, and correspondingly, the “single” and “last of many” echoes were pooled into a dataset denoted as “last” echoes.

[TABLE 2]

2.5.3. LiDAR data processing

The entire study area was divided into grid cells using regular grids that were laid atop the stand map in a Geographical Information System (GIS) operation. For every grid cell, canopy height distributions were derived from the LiDAR echoes within the respective cells. Order statistics from these distributions are among the LiDAR metrics we derived, see below. Because order statistics are a monotone increasing function of sample size and thus spatial scale (Harter, 1970; Magnussen, 1999), it is important that grid cell size and size of the sample survey plots are equal to avoid unequal expectations of the metrics derived from the height distributions. Thus, we used a grid cell size of 200 m^2 and these cells represented the elements that constituted our population, see details below. In total, the population consisted of 26,135 such cells.

Separate distributions were created for the first and last echoes of the 1999 and 2010 LiDAR data, respectively. A threshold value of 1.3 m above the ground surface was used to separate the ground echoes from those belonging to the relevant parts of the tree layer/tree canopy. From each of these two distributions and for every grid cell we extracted order statistics such as height percentiles. Further, we derived multiple measures of canopy density. The canopy density measures were derived by dividing the height range between the 1.3 m threshold and the 95 percentile into 10 equally sized height bins. The densities were then computed as the respective ratios between number of echoes above a given height bin and total number of echoes (including the below-canopy echoes). Thus, the canopy density measures represent the relative cumulative frequencies of echoes from the top of the canopy at different heights levels in the canopy.

Differences between corresponding variables as derived from the 2010 and 1999 data, respectively, were also computed, such as for example the difference between a given height percentile in 2010 and in 1999. Similarly, we also computed the ratios between corresponding variables from 2010 and 1999.These differences and ratios in LiDAR variables as well as the primary LiDAR variables derived directly from the 1999 and 2010 acquisitions were used as auxiliary information in the estimation. Finally, we derived the same LiDAR variables for every sample survey plot as for the grid cells.

2.6. Classification according to type of change (management activity)

When post-stratification is used in forest inventories one is often concerned with a description of the current state of the land, for example the current land use (e.g. forest versus non-forest) or the current state of the forest (e.g. age and tree species). In this study however, we address estimation of changes in biomass. Consequently, we would be interested in a post-stratification that eventually could improve the precision of the change estimates and where the individual post-strata themselves are relevant reporting units for the management activities causing the changes. We would therefore seek a post-stratification that reflects the changes between two observations in time rather than the state at a given point in time.

Several types of changes in a forest landscape may merit attention and LiDAR may prove useful for identifying such changes. First, we wanted to address areas subject to a complete loss of tree biomass. In a managed boreal forest, that could be interpreted as a recent clear-felling. In a tropical forest, i.e., in a REDD context, such changes could represent deforestation. Further, we wanted to address areas subject to a partial and temporary loss of tree biomass. In a boreal context, that could be interpreted as a thinning or a shelterwood cutting while in a tropical forest such losses would indicate forest degradation. Finally, we wanted to identify areas with a stable or increasing biomass, i.e., areas subject to natural processes such as continuous growth and natural mortality. Thus, we identified three mutually exclusive and non-overlapping change categories.

These categories were treated as post-strata in the estimation. Thus, we will use the term "post-stratum" for each of these categories and they may be characterized in the following way:

Post-stratum A: "Deforestation" or "recently clear-felled".

Post-stratum B: "Degradation" or "thinning or shelterwood cutting".

Post-stratum C: "Untouched".

Our first task was to assign one of these unique post-strata to each individual sample survey plot. We did not make specific observations of change category during field work, but rather assigned post-stratum to the field sample plots according to simple classification rules based on the biophysical field data. These simple rules are shown in Table 3. They are based on observed plot biomass and stem number in 1999 and 2010. In order to be meaningful, some of the rules differed between forest classes for a given post-stratum.

[TABLE 3]

Second, we needed to classify every individual element (grid cells with size 200 m^2) of the entire population so that they could be assigned to the mutually exclusive post-strata. For this purpose we fitted a logistic regression model with the three post-strata as the categorical response variable and LiDAR metrics as independent variables. The fitted model was subsequently used to predict the post-stratum to be assigned to every population element (grid cell) using the LiDAR metrics of the individual cells as independent variables. A similar strategy has been proposed by McRoberts (2011) for classifying forest types using Landsat TM data as independent variables.

In the logistic regression analysis, a multinomial model of the probability of the three post-strata assuming nominal classes, i.e., unordered classes, was fitted. The modeling was based on the 176 sample survey plots. In the analysis we sought LiDAR metrics as independent variables which we anticipated could characterize the changes in canopy height and canopy density. Thus, we selected the three upper height percentiles (*pf*70, *pf*80, *pf*90) and the three lower canopy densities (*df*0, *df*1, *df*2) of the first echo LiDAR data from 1999 and 2010, and calculated the differences between corresponding metrics from 2010 and 1999 ($\delta pf70$, $\delta pf80$, $\delta pf90$, $\delta df0$, $\delta df1$, $\delta df2$). We fitted logistic regression models for different combinations of pairs with one variable selected among each of the two types of variables, i.e., height-related and density-related metrics, respectively.

In multinomial logistic regression, the probabilities are jointly estimated as one system. The probability of each post-stratum is estimated relative to the probability of a chosen baseline post-stratum. In the estimation, post-stratum A (deforestation) was chosen as the baseline post-stratum. Thus, for the other post-strata (i.e., post-strata B and C) the probabilities of post-stratum j (p_{B} and p_{C}) were estimated according to the following multinomial logistic regression model:

$$\log\left(\frac{p_j}{1-p_{\mathrm{A}}}\right)=\alpha_j+\beta_{1j}\delta pf+\beta_{2j}\delta df+\varepsilon \qquad (1)$$

where δpf is a difference between height percentiles and δdf is a difference between canopy densities. Maximum-likelihood computation was applied for fitting the model in Eq. (1). The logistic regression procedure of the SAS package (Anon., 2004) was used. There is no obvious choice for a single goodness-of-fit statistic for multinomial logistic regression, although some tests have been proposed lately (e.g. Pigeon & Heyse, 1999; Goeman & Le Cessie, 2006). In this study, deviance and Pearson chi-square goodness-of-fit statistics are reported. The goodness-of-fit of the models was also assessed by leave-one-out cross validation. For subsequent prediction for each population element we selected the model with the highest overall accuracy in the cross validation and which otherwise satisfied the goodness-of-fit statistics mentioned above.

A unique post-stratum for each element of the population was assigned according to a deterministic approach, i.e., by choosing the outcome with the highest predicted probability among the three post-strata. The probabilities of the three mutually exclusive outcomes were predicted according to

$$p_j=\frac{\exp\left(\alpha_j+\beta_{1j}\delta pf+\beta_{2j}\delta df\right)}{1+\sum_q \exp\left(\alpha_q+\beta_{1q}\delta pf+\beta_{2q}\delta df\right)} \qquad (2)$$

for the q non-baseline post-strata B and C and according to Eq. (3) for the baseline post-stratum (post-stratum A), i.e.,

$$p_{\mathrm{A}} = \frac{1}{1+\sum_{q}\exp\left(\alpha_q + \beta_{1q}\delta pf + \beta_{2q}\delta df\right)} \tag{3}$$

2.7. Estimators

The current study was based on a (pre-) stratified sample survey. However, sample surveys intended for e.g. estimation of current resources will frequently follow stratification criteria other than those found relevant for change estimation. Furthermore, sample surveys designed specifically for change estimation, for example for local REDD projects, will most likely profit from a stratification allowing a more intensive sampling in areas expected to be subject to future changes in carbon stocks (e.g. along deforestation frontiers) in order to improve precision of the change estimates (Stehman, 2009). Such initial strata cannot be expected to match perfectly with post-strata resulting from a *posteriori* classification of actual changes.

In the following, our first objective was to estimate the areal proportion of each of the post-strata reflecting different management activities (see above) assuming a stratified design, and subsequently the total area of each post-stratum. Second, we wanted to estimate the net change in biomass for each of the post-strata and subsequently the net change in biomass for the entire AOI. The current setting with an initial stratification and post-stratification is highly relevant to real world survey designs.

2.7.1. Estimation of areal proportions based on the field sample survey

We wanted to estimate the areal proportion of each post-stratum. Adopting the notation of Särndal et al. (1992), let U be the entire population of elements (grid cells with size 200 m^2) in the AOI where $U=\{1, ..., k, ..., N\}$. This population is divided into H non-overlapping pre-strata. The pre-strata are denoted U_h . The sizes of the pre-strata (number of population elements) are N_h , where $h=1, ..., H$.

Now, let I_k^g be an indicator of post-stratum g, g=1, …, G, of the kth element in the population such that

$$I_k^g = \begin{cases} 1, \text{ if the } k\text{th element belongs to post-stratum } g \\ 0, \text{ otherwise} \end{cases}$$

First, we want to define the proportion of the area in a particular post-stratum (g) within a pre-stratum (h). We define this proportion (P_h^g) for which we wish to find an appropriate estimator as

$$P_h^g = \frac{\sum_{k \in U_h} I_k^g}{N} = \frac{N_h^g}{N} \ , \qquad (4)$$

where N_h^g is the total number of population elements in pre-stratum h classified as post-stratum g.

We may estimate the areal proportion from the field sample alone, i.e., using a so-called direct estimator. Let s be our sample of field survey plots and let s_h denote a subsample of size n_h drawn randomly from the elements in U_h , i.e., from stratum h. Thus, s constitutes a stratified random sample (STRS). Following Cochran (1977, p. 107), the proportion of the population area in a particular post-stratum g within pre-stratum h was estimated according to

$$\hat{P}_{\text{STRS}h}^g = \frac{N_h}{N} \ \frac{\sum_{k \in s_h} I_k^g}{n_h} = \frac{N_h}{N} \ \frac{n_h^g}{n_h} \ , \qquad (5)$$

where n_h^g is the number of sample plots in stratum h classified as post-stratum g. A variance estimator of $\hat{P}_{\text{STRS}h}^g$ (Cochran, 1977, p. 108) is given by

$$\hat{V}\left(\hat{P}_{\text{STRS}h}^g\right) = \left(1 - \frac{n_h}{N_h}\right)\left(\frac{N_h}{N}\right)^2 \ \frac{\frac{n_h^g}{n_h}\left(1 - \frac{n_h^g}{n_h}\right)}{n_h - 1} \ \approx \left(\frac{N_h}{N}\right)^2 \ \frac{\frac{n_h^g}{n_h}\left(1 - \frac{n_h^g}{n_h}\right)}{n_h - 1} \ . \qquad (6)$$

Note that in this estimator and in all subsequent variance estimators we will ignore the so-called “finite population term” because the sampling fractions are always very small and their influence on the variance estimates would be negligible in our applications.

Now, for a particular post-stratum g, the areal proportion was estimated following standard stratified sampling:

$$\hat{P}^{g}_{\mathrm{STRS}} = \sum_h \hat{P}^{g}_{\mathrm{STRS}h} \tag{7}$$

with the variance estimator

$$\hat{V}\left(\hat{P}^{g}_{\mathrm{STRS}}\right) = \sum_h \hat{V}\left(\hat{P}^{g}_{\mathrm{STRS}h}\right) \ . \tag{8}$$

For a direct comparison with the estimators given in Cochran (1977) it should be noted that while we give the estimators for the proportion of area of each post-stratum within a given pre-stratum in Eq. (5) and the corresponding variance estimator in Eq. (6) and subsequently the estimators for the proportion of area of each post-stratum across all pre-strata in Eq. (7) and the corresponding variance estimator in Eq. (8), Cochran (1977) gave the two latter estimators directly (Eq. 5.52 and Eq. 5.56) without explicitly presenting the within pre-strata estimators.

2.7.2. Estimation of areal proportions based on the field sample survey and auxiliary LiDAR data

The logistic regression model was used to provide predictions of post-stratum for every population element (200 m^2 grid cell). This information can be treated as auxiliary to the field data in the estimation and thus potentially help to improve the precision of the estimators for areal proportions and areas of the post-strata. The probability-based design of the survey allowed adoption of a model-assisted estimator. In model-assisted estimators, predictions are used for a fairly large sample of population elements (or even all population elements as in the current study) to provide a pure model-based estimate of the population parameter of interest. This estimate is adjusted for deviations between the model predictions and the observed values in the sample. Thus, model-assisted estimators are design-unbiased or approximately design-unbiased (Särndal et al., 1992, p. 227). When a sample for a large area is used to provide estimates for a smaller area based on predictions, as is the case in this study since we developed predictive logistic regression models for post-strata across several pre-strata and used that global model to predict post-stratum for each individual pre-stratum, an estimator based on pure predictions for the smaller area (pre-stratum) is known as a synthetic estimator.

In the current study, we adopted a model-assisted generalized regression estimator (Särndal, 2011). In a remote sensing study by McRoberts (2010) a so-called difference estimator (Särndal et al., 1992, p. 221-225) was adopted for the same purpose. Let $\hat{I}_k^g$ be an indicator of the predicted post-stratum g of the kth element in the population defined in the same way as I_k^g above, with the only difference being that $\hat{I}_k^g$ is an indicator of the predicted post-stratum while I_k^g was an indicator of the observed post-stratum. Thus, the synthetic (SYNT) estimator for P_h^g is

$$\hat{P}_{\mathrm{SYNT}h}^g = \frac{\sum_{k \in U_h} \hat{I}_k^g}{N} = \frac{N_h}{N} \frac{\sum_{k \in U_h} \hat{I}_k^g}{N_h} \ , \tag{9}$$

whereas the model-assisted generalized regression (MAR) estimator for the proportion of the population area in a particular post-stratum g within pre-stratum h is

$$\hat{P}_{\mathrm{MAR}h}^g = \frac{N_h}{N} \left(\frac{\sum_{k \in U_h} \hat{I}_k^g}{N_h} + \frac{\sum_{k \in s_h} \hat{e}_k^g}{n_h} \right), \tag{10}$$

where $\hat{e}_k^g = I_k^g - \hat{I}_k^g$. A variance estimator of $\hat{P}_{\mathrm{MAR}h}^g$ is

$$\hat{V}\left(\hat{P}_{\mathrm{MAR}h}^g\right) = \left(\frac{N_h}{N}\right)^2 \ \frac{\sum_{k \in s_h} \left(\hat{e}_k^g - \bar{\hat{e}}_k^g\right)^2}{n_h(n_h - 1)} \quad , \tag{11}$$

where $\bar{\hat{e}}_k^g$ is the arithmetic mean of the residuals ($\hat{e}_k^g$) of the n_h elements in the sub-sample s_h. As noted by Mandallaz (2008, p. 120), the synthetic component of the estimator, i.e., the first term in the brackets on the right-hand side of the estimator in Eq. (10), does not contribute to the design-based variance, and thus the variance only depends on the sample size and the goodness of the model for use in a particular pre-stratum (Särndal, 1984).

For a particular post-stratum g, the areal proportion was estimated according to the model-assisted approach following standard stratified sampling:

$$\hat{P}^{g}_{\mathrm{MAR}} = \sum_{h} \hat{P}^{g}_{\mathrm{MAR}h} \tag{12}$$

with the variance estimator

$$\hat{V}\left(\hat{P}^{g}_{\mathrm{MAR}}\right) = \sum_{h} \hat{V}\left(\hat{P}^{g}_{\mathrm{MAR}h}\right) \ . \tag{13}$$

Finally, the total area $\hat{A}^{g}$ in hectares of each post-stratum g in the AOI and the associated variance $\hat{V}\left(\hat{A}^{g}\right)$ were estimated for the direct (STRS; $\hat{P}^{g}_{\mathrm{STRS}}$) as well as the model-assisted (MAR; $\hat{P}^{g}_{\mathrm{MAR}}$) approaches according to

$$\hat{A}^{g} = \frac{200}{10000} N \hat{P}^{g} \tag{14}$$

where 200/10000 is used to scale from 200 m^2 estimates (the size of the population elements and sample plots) to per hectare estimates, and

$$\hat{V}\left(\hat{A}^{g}\right) = \left(\frac{200}{10000} N\right)^{2} \hat{V}\left(\hat{P}^{g}\right) , \tag{15}$$

respectively. Here $\hat{P}^{g}$ is used as a common symbol for $\hat{P}^{g}_{\mathrm{STRS}}$ as well as for $\hat{P}^{g}_{\mathrm{MAR}}$.

2.7.3. Estimation of change in biomass based on the field sample survey

In the following, we wanted to estimate the net change in biomass for each post-stratum and for the entire AOI and subsequently the variance of these change estimates. In the following we will condition the estimation on the actual post-stratification obtained with the logistic regression model. Although misclassification of post-strata will introduce errors, the only effect of erroneous classification on the biomass change estimates is an eventual decreased precision (reduced efficiency of the post-stratification).

We need to extend the notation to account for post-stratification in addition to the initial stratification. Thus, let the H non-overlapping pre-strata now be denoted $U_{\cdot h}$ with sizes $N_{\cdot h}$, where

h=1, ..., H. By post-stratification we also divide the population into non-overlapping post-strata $U_{g\cdot}$ with sizes $N_{g\cdot}$, where g=1, ..., G. Thus, with G post-strata intersecting the H pre-strata the AOI is partitioned into a maximum of G×H unique groups defined by post-stratum and pre-stratum. These groups are labelled U_{gh} with sizes N_{gh} .

Let δb_k be the change in biomass of the kth unit in the population. First, we want to define the parameter net change in biomass (ΔB) within a particular post-stratum (g) and pre-stratum (h) for which we later wish to find an appropriate estimator:

$$\Delta B_{gh} = \sum_{k\in U_{gh}} \delta b_k \quad . \tag{16}$$

We will first estimate net change in biomass from the field sample alone assuming stratified random sampling (STRS) followed by post-stratification. An Horvitz-Thompson (HT) estimator of $\Delta B_{gh}$is (Särndal et al., 1992, p. 268)

$$\widehat{\Delta B}_{\text{STRS-HT}gh} = \sum_{k\in s_{gh}} \frac{\delta b_k}{\pi_k} = N_{\cdot h} \frac{n_{gh}}{n_{\cdot h}} \overline{\delta b}_{gh} \tag{17}$$

for $\pi_k = n_{\cdot h}/N_{\cdot h}$ (Särndal et al., 1992, p. 31) where $\overline{\delta b}_{gh}$ is the arithmetic mean of the change in biomass of the n_{gh} elements in the sub-sample s_{gh} (Särndal et al., 1992, p. 269). Furthermore, an HT estimator of $\Delta B_{g\cdot}$ is (the numerator in Eq. 7.6.7 in Särndal et al., 1992, p.268)

$$\widehat{\Delta B}_{\text{STRS-HT}g\cdot} = \sum_h \widehat{\Delta B}_{\text{STRS-HT}gh} \quad , \tag{18}$$

while HT estimators of the sizes of post-stratum and pre-stratum gh and post-stratum g, respectively, are

$$\hat{N}_{\text{STRS-HT}gh} = \sum_{k\in s_{gh}} \frac{1}{\pi_k} = N_{\cdot h} \frac{n_{gh}}{n_{\cdot h}} \tag{19}$$

and

$$\hat{N}_{\text{STRS-HT}g\cdot} = \sum_h \hat{N}_{\text{STRS-HT}gh} \quad . \tag{20}$$

Thus, for post-stratum g we have the following estimator of net change in biomass (Särndal et al., 1992, p. 268)

$$\widehat{\Delta B}_{\text{STRS}g\cdot} = \frac{N_{g\cdot}}{\hat{N}_{\text{STRS-HT}g\cdot}} \widehat{\Delta B}_{\text{STRS-HT}g\cdot} \; . \tag{21}$$

The adjustment of $\widehat{\Delta B}_{\text{STRS-HT}g\cdot}$ by the ratio of known to estimated post-stratum size serves to improve the precision of $\widehat{\Delta B}_{\text{STRS}g\cdot}$ compared to that of $\widehat{\Delta B}_{\text{STRS-HT}g\cdot}$. An estimator of net change in biomass for the entire AOI is

$$\widehat{\Delta B}_{\text{STRS}} = \sum_g \widehat{\Delta B}_{\text{STRS}g\cdot} \; . \tag{22}$$

Now, let us proceed with the variance estimation, which we condition on the realized sample size in a post-stratum (n_{gh}). Conditionally on n_{gh}, $\hat{N}_{\text{STRS-HT}gh}$ and $\hat{N}_{\text{STRS-HT}g\cdot}$ are constants. We therefore have (Särndal et al., 1992, p. 288)

$$\hat{V}\left(\widehat{\Delta B}_{\text{STRS-HT}gh} | n_{gh}\right) = N_{gh}^2 \frac{\sum_{k \in s_{gh}} \left(\delta b_k - \overline{\delta b}_{gh}\right)^2}{n_{gh}(n_{gh}-1)} \quad . \tag{23}$$

As in the previous sections, we have ignored corrections for finite population.

For a particular post-stratum g we have the variance estimator

$$\hat{V}\left(\widehat{\Delta B}_{\text{STRS}g\cdot} | n_{g1}, \ldots, n_{gH}\right) = \left(\frac{N_{g\cdot}}{\hat{N}_{\text{STRS-HT}g\cdot}}\right)^2 \sum_h \hat{V}\left(\widehat{\Delta B}_{\text{STRS-HT}gh} | n_{gh}\right) \quad , \tag{24}$$

whereas for the entire AOI the variance was estimated according to

$$\hat{V}\left(\widehat{\Delta B}_{\text{STRS}} | n_{11}, \ldots, n_{GH}\right) = \sum_g \hat{V}\left(\widehat{\Delta B}_{\text{STRS}g\cdot} | n_{g1}, \ldots, n_{gH}\right) \; . \tag{25}$$

Because a systematic design was adopted for the field survey rather than a random design, an overestimation of the variance is a likely consequence of ignoring the systematic design (e.g. Särndal et al., 1992).

2.7.4. Estimation of change in biomass based on the field sample survey and auxiliary LiDAR data

In the same manner as we took advantage of the LiDAR data for all population elements as auxiliary information in the estimation of areal proportions, we will now utilize the LiDAR data for every element of the population to assist the estimation of net change in biomass for each post-stratum and for the entire AOI. We started by obtaining synthetic estimates of change in biomass for every population element using a synthetic regression estimator (Särndal et al., 1992). For a particular post-stratum and pre-stratum this estimator can be formulated as

$$\widehat{\Delta B}_{\mathrm{SYNT}gh} = \sum_{k \in U_{gh}} \widehat{\delta b}_k \qquad (26)$$

where $\widehat{\delta b}_k$ is change in biomass predicted according to a regression model for the *k*th element (200 m^2 grid cell) in the population as opposed to the observed change in biomass (δb_k) as defined above. In the current study, three different approaches to post-stratum specific modeling and prediction of change in biomass based on a few selected variables derived from the LiDAR measurements were employed, see further details below. We accounted for any potential bias inherent in the synthetic estimator by employing a model-assisted approach. Drawing upon the probability-based principles on which the field sample was selected, we used a model-assisted generalized regression (MAR) estimator (Särndal et al., 1992, p. 231; Särndal, 2011). For net change in biomass for a particular post-stratum (g) and pre-stratum (h), a model-assisted regression estimator is

$$\widehat{\Delta B}_{\mathrm{MAR}gh} = \sum_{k \in U_{gh}} \widehat{\delta b}_k + \sum_{k \in s_{gh}} \frac{\hat{e}_k}{\pi_k} \quad , \qquad (27)$$

where we have $\pi_k = n_{\cdot h}/N_{\cdot h}$ as before and $\hat{e}_k = \delta b_k - \widehat{\delta b}_k$. Thus,

$$\widehat{\Delta B}_{\mathrm{MAR}gh} = \sum_{k\in U_{gh}} \widehat{\delta b}_k + N_{\cdot h}\frac{n_{gh}}{n_{\cdot h}}\bar{\hat{e}}_{gh} \ , \tag{28}$$

where $\bar{\hat{e}}_{gh}$ is the arithmetic mean of the residuals of the n_{gh} elements in the sub-sample s_{gh} .This estimator is approximately design-unbiased irrespective of the model choice when the sample size is not too small. It allows for use of different types of models for the synthetic component, such as e.g. non-linear regression models (Särndal, 2011).

Correspondingly, a model-assisted regression estimator for post-stratum g is

$$\widehat{\Delta B}_{\mathrm{MAR}g\cdot} = \sum_{k\in U_{g\cdot}} \widehat{\delta b}_k + \frac{N_{g\cdot}}{\hat{N}_{\text{STRS-HT}g\cdot}}\sum_h N_{\cdot h}\frac{n_{gh}}{n_{\cdot h}}\bar{\hat{e}}_{gh} \tag{29}$$

and for the entire AOI

$$\widehat{\Delta B}_{\mathrm{MAR}} = \sum_g \widehat{\Delta B}_{\mathrm{MAR}g\cdot} \ . \tag{30}$$

A variance of $\widehat{\Delta B}_{\mathrm{MAR}gh}$ conditioned on the realized sample size in a given post-stratum (n_{gh}) is (Särndal et al., 1992, p. 246, 288)

$$\hat{V}\left(\widehat{\Delta B}_{\mathrm{MAR}gh}|n_{gh}\right) = N_{gh}^2\frac{\sum_{k\in s_{gh}}\left(\hat{e}_k-\bar{\hat{e}}_k\right)^2}{n_{gh}(n_{gh}-1)} \ . \tag{31}$$

When working with small units such as the $G\times H$ groups, there is a risk of fairly small samples (n_{gh}). The variance estimator is unbiased only asymptotically and may not be unbiased for very small samples. It has been indicated that samples smaller than five (Thompson, 2002) or 10 (Särndal et al., 1992) should be avoided.

For a particular post-stratum g we have the variance estimator

$$\hat{V}\left(\widehat{\Delta B}_{\mathrm{MAR}g\cdot}|n_{g1},\dots,n_{gH}\right) = \left(\frac{N_{g\cdot}}{\hat{N}_{\text{STRS-HT}g\cdot}}\right)^2\sum_h \hat{V}\left(\widehat{\Delta B}_{\mathrm{MAR}gh}|n_{gh}\right) , \tag{32}$$

whereas for the entire AOI the variance was estimated according to

$$\hat{V}\left(\widehat{\Delta B}_{\mathrm{MAR}} | n_{11}, \ldots, n_{GH}\right) = \sum_g \hat{V}\left(\widehat{\Delta B}_{\mathrm{MAR}g\cdot} | n_{g1}, \ldots, n_{gH}\right) . \quad (33)$$

Finally, mean change in biomass per hectare for each post-stratum g ($\hat{\lambda}_{g\cdot}$) and in the entire AOI ($\hat{\lambda}$) and the associated variances were estimated for the direct (STRS) as well as the model-assisted (MAR) approaches according to

$$\hat{\lambda}_{g\cdot} = \frac{1}{\frac{200}{10000} N_{g\cdot}} \widehat{\Delta B}_{g\cdot} , \quad (34)$$

$$\hat{\lambda} = \frac{1}{\frac{200}{10000} N} \widehat{\Delta B} , \quad (35)$$

$$\hat{V}\left(\hat{\lambda}_{g\cdot}\right) = \frac{1}{\left(\frac{200}{10000} N_{g\cdot}\right)^2} \hat{V}\left(\widehat{\Delta B}_{g\cdot} | n_{g1}, \ldots, n_{gH}\right) , \quad (36)$$

and

$$\hat{V}\left(\hat{\lambda}\right) = \frac{1}{\left(\frac{200}{10000} N\right)^2} \hat{V}\left(\widehat{\Delta B} | n_{11}, \ldots, n_{GH}\right) , \quad (37)$$

respectively. Here $\widehat{\Delta B}_{g\cdot}$ and $\widehat{\Delta B}$ are used as common symbols for the STRS and MAR estimators (the STRS and MAR subscripts are ignored).

As noted above, the estimation was conditioned on the actual post-stratification obtained with the logistic regression model. Although misclassification of post-strata will introduce errors in the areal estimates, the only effect of erroneous classification on the biomass change estimates per hectare is an eventual decreased precision.

2.8. Modeling of change in biomass

Regression models that relate the LiDAR variables to change in above-ground biomass are required for the model-assisted estimation. In this study, biomass was determined on each field sample plot for two points in time. We could therefore estimate change in biomass directly on each field plot and consequently also model change in biomass directly. Several approaches to modeling of change in biomass may merit attention. Bollandsås et al. (2012) tested different approaches when modeling change in biomass with airborne LiDAR data. In the current study, three particular approaches were followed, namely (A) direct modeling of net change in biomass, i.e., using δAGB as a response variable (denoted approach A) and (B) separate modeling of (*i*) biomass in 1999 (AGB_{1999}) and (*ii*) the ratio of biomass in 2010 (AGB_{2010}) to biomass in 1999 (AGB_{1999}) (denoted approach B). The change in biomass could then be predicted as the product of predicted biomass in 1999 and predicted ratio minus the predicted biomass in 1999. Finally, (C) separate modeling of (*i*) biomass in 1999 (AGB_{1999}) and (*ii*) biomass in (AGB_{2010}) was carried out (denoted approach C). In this latter approach the change in biomass could be predicted as the difference between predicted biomass in 2010 and predicted biomass in 1999.

2.8.1. Direct modeling of change in biomass (approach A)

For direct modeling of net change in biomass a simple multiple linear regression model form was used because this model form allows positive as well as negative values of the response. Thus, we estimated the mean (expected value) function according to

$$\mathrm{E}[\delta AGB] = \beta_0 + \mathbf{X}\beta \quad , \tag{38}$$

where β_0 is a constant term, β is a vector of regression coefficients, and $\mathbf{X}$ is a matrix of explanatory LiDAR variables such as the differences in (1) corresponding height percentiles, (2) corresponding canopy densities, (3) corresponding mean values, and (4) corresponding standard deviations and coefficients of variation between the two points in time for first and last echo data.

Six different models were fitted. First, we fitted a separate model for those field plots that according to predictions obtained with the logistic regression model were classified to belong to post-stratum A (deforestation). Second, we fitted a model to the plots classified as post-stratum B (degradation). Finally, we fitted four different models for plots in post-stratum C (untouched), i.e., one model for each of the four predefined forest classes within post-stratum C. The six models were fitted with the ordinary least-squares method (OLS) and stepwise variable selection using the SAS statistical software package (Anon., 2004).

2.8.2. Modeling of change in biomass by a system of models (approach B)

A multiplicative model form was adopted for modeling of biomass in 1999 (AGB_{1999}) as well as for modeling of the ratio between biomass in 2010 and 1999 (AGB_{2010}/AGB_{1999}). We used nonlinear regression (the Gauss-Newton method; Anon., 2004) to estimate nonlinear models of the mean (expected value) function. These models were of the form

$$\mathrm{E}\,[Y] = \beta_0 x_1^{\beta_1} x_2^{\beta_2} \ldots x_m^{\beta_m} \quad , \tag{39}$$

where $Y = AGB_{1999}$ or AGB_{2010}/AGB_{1999} field values, $x_1, x_2, \ldots, x_m$ are the LiDAR-derived variables and $\beta_0, \beta_1, \beta_2, \ldots, \beta_m$ are parameters to be estimated. When AGB_{1999} was the response variable, the LiDAR-derived variables were the height percentiles and canopy densities derived from the 1999 LiDAR data. When the ratio AGB_{2010}/AGB_{1999} was the response variable, the LiDAR-derived variables were the corresponding ratios of the height percentiles and canopy densities derived from the 1999 and 2010 LiDAR data. Six separate sets of models were fitted, i.e., for the six subsets of plots indicated above. In order to select among the large number of potential LiDAR variables to be included as explanatory variables in the final models, we carried out a preliminary estimation of log-transformed models using OLS regression and took advantage of the stepwise (forward) selection procedure, see further details in Næsset et al. (2011). It should be noted that for each set of models the specific models for biomass in 1999 and the ratio between the biomass in 2010 and 1999 were estimated independently because we wanted to keep the analysis simple and focus on the application rather than on specifics of the estimation techniques. Methods like for example seemingly unrelated regression or partial least squares regression which have previously been applied to LiDAR data (Næsset et al., 2005) could have been considered though.

2.8.3. Modeling of change in biomass by separate models for each point in time (approach C)

In addition to the models fitted for AGB_{1999} (see above) we also fitted models for AGB_{2010} following the same model form (Eq. 39). Six separate models with AGB_{2010} as response variable were fitted for exactly the same subsets of plots as used for the AGB_{1999} models.

2.9. Estimation

2.9.1. Estimation of changes in areas and corresponding variances

First, we estimated the total area of each post-stratum (Eqs. 7 and 14) from the field sample only. The classification of change (i.e. post-stratum) on the field plots followed the simple classification rules (Table 3). We also estimated the corresponding standard errors (SE), i.e., the square roots of the variances (Eqs. 8 and 15).

Second, model-assisted estimates of total area of each post-stratum (Eqs. 12 and 14) with the LiDAR data used as auxiliary information were obtained. The auxiliary information was used with the fitted logistic regression model to predict post-stratum for each element in the population. Separate estimates of the synthetic component (i.e., pure model-based predictions) of the model-assisted estimates were also provided. Finally, we estimated standard errors for the model-assisted estimates (Eqs. 13 and 15).

2.9.2. Estimation of change in biomass and corresponding variances

Change in biomass per hectare for each individual post-stratum (Eqs. 21 and 34) and corresponding standard errors (Eqs. 24 and 36) were estimated from the field sample only. The post-strata for all population elements, including the plots, were determined by the logistic regression model predictions. The assignment of the plots to post-strata was based on the plots' predicted post-strata. Estimates of change in biomass per hectare for the entire AOI (Eqs. 22 and 35, respectively) and corresponding standard error estimates were provided as well (Eqs. 25 and 37).

We also estimated change in biomass per hectare for each individual post-stratum according to the model-assisted approach (Eqs. 29 and 34) using the LiDAR model predictions of change in biomass for every population element to support the estimation. The adjustment for bias in the model-assisted estimators was undertaken by estimating the residuals ($\hat{e}_k$) for the plots in accordance with previously established practice (Gregoire et al., 2011, p. 93). Alternative estimates were provided using the simple linear regression models for change (Eq. 38 and Table 6), the ratio approach (Eq. 39 and Table 6), and separate models for *AGB* in 1999 and 2010 (Eq. 39 and Table 6). Corresponding standard error estimates were provided (Eqs. 32 and 36). The synthetic components of the change estimates were given separately. During estimation, we inspected the pure model predictions at a population element level. For the ratio approach (approach B) we noticed predicted values of the ratio between *AGB* in 2010 and 1999 for category A (deforestation) corresponding to an increase in biomass over the 11-year period of 19,500 Mg ha^{-1}. The maximum observed biomass in the field sample was 462.3 Mg ha^{-1} (Table 1). To avoid such completely unrealistic predictions we introduced an upper limit on allowable predictions of the ratio for this particular category. This limit was set to 1 and thus allowing a stable biomass over the observation period.

Finally, model-assisted estimates of change in biomass for the entire population (Eqs. 30 and 35) and their standard error estimates (Eqs. 33 and 37) were obtained following all three modeling approaches.

3. Results and discussion

3.1. Model fitting

3.1.1. Models for prediction of post-stratum (type of change)

The multinomial logistic regression model for prediction of post-stratum that resulted in the best overall classification accuracy in a leave-one-out cross validation consisted of the difference between the 70th height percentiles of the 2010 and 1999 LiDAR data ($\delta pf70$) and the corresponding difference for the cumulative canopy density at 1.3 m above ground ($\delta df0$) as explanatory variables. The regression coefficient estimates indicated that relative to the deforestation post-stratum, the probabilities of degradation and untouched increased with increasing positive changes in height as well as canopy density over the 1999 to 2010 time span (Table 4). This pattern was more pronounced for untouched than for degradation, which is reasonable. Four of the six estimated regression coefficients were statistically significant at the 5 percent level. Thus, the fitted model demonstrated that time series of LiDAR data are able to describe a logical relationship between types of changes in a forest landscape and changes in heights and canopy density. Also the goodness-of-fit statistics (Table 4) revealed a good model fit as did the overall classification accuracy of the cross validation. The overall accuracy was 93.8% (Table 5).

[TABLE 4]

The cross validation revealed high classification accuracies for the post-strata deforestation and untouched (95.7-97.8%). The lower user's and producer's accuracies for the degradation post-stratum (56.3-69.2%) were mainly caused by confusion with the untouched post-stratum. However, an inspection of the six omissions predicted to be untouched (Table 5) revealed that the field data in fact showed an increase in biomass from 1999 to 2010 but also a reduction in stem number. Thus, the sensitivity of the LiDAR data to capture changes in biomass actually seemed to work quite well but at the same time the LiDAR data failed to capture a reduction in stem number. The somewhat weaker correlation between LiDAR metrics and stem number is well known (Næsset, 2007).

The confusion between the deforestation and degradation post-strata (omission as well as commission) was somewhat surprising, given the clear expectation of airborne LiDAR being highly sensitive to a severe loss of biomass, which was used as a field-based criterion for defining the post-stratum deforestation (Table 3). To learn why some of the sample plots were misclassified as shown in the error matrix (Table 5), we revisited a few selected plots in field on 25 January 2012. As an example, the single plot observed to be deforested and erroneously predicted to be degraded will be mentioned (plot #33). During field work in 2010 we recorded heights of 13 sample trees on plot #33. The heights ranged between 0.5 and 4.0 m. Observed biomass in 2010 was 7.1 Mg ha^{-1} whereas it was188.9 Mg ha^{-1} in 1999. However, the LiDAR data for this plot showed laser heights with values up to 22.4 m even in 2010, indicating fairly large amounts of biomass. The field inspection revealed that there was a tall tree standing on the plot circumference with the center of the stem right outside the plot. Thus, this tree was correctly ignored during field work in 2010. However, about half the tree crown was hanging over the plot and the laser measurements for this part of the crown were included as auxiliary data for the plot (Fig. 2). As can be seen in Fig. 2, even the stem position is indicated in the LiDAR data as three laser echoes have been reflected from the stem itself inside the plot circumference. This illustrates the extreme sensitivity of LiDAR to record minor details of the distributional patterns of biological material with high geographical precision. Such border effects can hardly be avoided, but their relative influence will decline with increasing plot sizes. Thus, it is likely that severe misclassification errors will be less pronounced for larger plots.

Finally, it should be emphasized that the simple classification rules applied to classify into post-strata (Table 3) may not fully capture the changes we intended to characterize. With other definitions of the three post-strata a LiDAR-based classifier may perform differently. The predicted post-strata for each individual element of the population that formed the basis for the model-assisted estimation of the areal changes and the subsequent post-stratification is displayed in Fig. 1. Overall, the simple LiDAR-based classification performed quite well. Most remote sensing techniques have difficulties with distinguishing between the activity-based change categories and identifying partial loss of biomass (degradation) seems to be a particular challenge where LiDAR may offer superior performance.

[TABLE 5]
[FIGURE 2]

3.1.2. Models for prediction of change in biomass

The selected linear models following approach A (direct modeling of change) consisted of one to four explanatory LiDAR variables and 40 to 98% of the variability in observed biomass was explained by the models (Table 6). All types of LiDAR metrics were present as explanatory variables and we could not observe any particular pattern regarding types of variables (e.g. difference in height percentiles or difference in canopy density metrics) that were included in the selected models. This is not very surprising given that the different models for change in biomass covered very different transitions – including thinning, clear-felling, clear-felling with subsequent planting or natural regeneration as well as forest stands left untouched for the entire 11 year period.

The multiplicative models for above-ground biomass in 1999 (approach B and C) and 2010 (approach C) contained one to two explanatory variables and explained 67 to 93% of the variability. All models with two variables (with one exception) contained one variable related to height (mean height or height percentile) and one related to canopy density. This is a logical result and well in line with previous findings (e.g. Næsset et al., 2011). The proportion of explained variability is also consistent with previous findings from boreal forests [cf. a brief summary presented in Næsset & Gobakken (2008)].

An interesting pattern was observed in the fitted multiplicative models for the ratio between biomass in 2010 and 1999. For the two models fitted in post-strata A and B (deforestation and degradation; R^2=0.92-0.95) only variables related to the ratio between canopy densities were included in the selected models whereas for all the four models (with one exception) in the untouched post-stratum (post-stratum C; R^2=0.44-0.87) ratios related to height percentiles as well as canopy densities were included. Thus, it appears that for dramatic changes such as complete or almost complete (deforestation) or partial (degradation) loss of biomass, relative canopy density is a powerful explanatory variable, which is reasonable. Removal of some or most of the trees consistently influences the density of the forest while the tree height (of the remaining trees) may be less influenced. For minor changes like continuous growth and natural mortality which influence on height as well as density the relative biomass between the two points in time is modeled in an appropriate way by the ratios of the same primary LiDAR variables as found suitable for modeling of the biomass itself.

[TABLE 6]

3.2. Estimation of changes in areas

The estimated area of deforestation based on the field survey (direct estimate) was 70.4 ha with a standard error of 14.5 ha (Table 7). Thus, a 95% confidence interval (*n*=23) for the deforested area would be approximately 40.4 to 100.4 ha. When the LiDAR data were used as auxiliary information to assist in the estimation the area of deforestation was 51.8 ha (SE=3.4). Because the total number of deforested field plots (based on the classification from the field data) was identical to the total number of plots predicted to be deforested following the logistic model predictions the estimated area based on pure model predictions (synthetic estimate) was identical to the model-assisted estimate.

For the degradation post-stratum the field-based areal estimate was 44.6 ha (SE=11.8 ha) whereas the model-assisted estimate was 53.4 ha (SE=6.7 ha). Aggregation of observations for population elements predicted to be degraded gave a synthetic estimate of 46.4 ha. The difference between the model-assisted and synthetic estimates was mainly caused by the confusion between the degradation and untouched post-strata in the logistic model predictions (Table 5). The estimated area of the untouched post-stratum was 407.7 (SE=17.4), 417.5 (SE=5.8), and 424.5 ha using the direct, model-assisted, and synthetic estimators, respectively (Table 7).

The results indicated fairly consistent estimates using the different estimators. However, the model-assisted estimates were much more precise than the field-based ones. The ratio between the estimated variances, also known as relative efficiency, ranged between 3.1 and 18.2, indicating that 3.1-18.2 as many field plots would be needed to achieve the same precision for a pure field-based estimate as obtained when assisting the estimation with LiDAR data. This assumes a simple random and unstratified design. Although the design in this study was somewhat more complex, it illustrates the huge potential of LiDAR data to improve precision of area change estimates for activity categories that would be of great interest and relevance to REDD.

[TABLE 7]

3.3. Estimation of changes in above-ground biomass

The field-based estimate of loss in biomass for areas predicted to be deforested was 131.8 Mg ha^{-1} (SE=8.9 Mg ha^{-1}). The model-assisted estimate of the loss was 162.7 Mg ha^{-1} (SE=5.8 Mg ha^{-1}) when linear models for change in biomass were applied and 158.0 Mg ha^{-1} (SE=4.9 Mg ha^{-1}) when a system of nonlinear models with the ratio approach was used to assist in the estimation. When two separate models for biomass in 1999 and 2010 were used the loss was 162.3 Mg ha^{-1} (SE=4.9

Mg ha^{-1}). The three alternative approaches to change modeling resulted in estimates of similar magnitude.

For the degradation post-stratum the direct estimate of loss in biomass was 45.9 Mg ha^{-1} (SE=31.1 Mg ha^{-1}) with model-assisted estimates of loss of 62.8 (SE=5.0 Mg ha^{-1}), 49.0 Mg ha^{-1} (SE=8.2 Mg ha^{-1}), and 52.2 Mg ha^{-1} (SE=8.4 Mg ha^{-1}), respectively. For the untouched post-stratum the differences in the estimates were even less pronounced, with a field-based estimate of gain in biomass of 43.1 Mg ha^{-1} (SE=2.8 Mg ha^{-1}) and corresponding model-assisted estimates following the three modeling approaches of 41.4 (SE=1.8 Mg ha^{-1}), 39.7 Mg ha^{-1} (SE=2.0 Mg ha^{-1}), and 42.4 Mg ha^{-1} (SE=2.3 Mg ha^{-1}), respectively. The overall net change in biomass for the entire AOI was estimated to 17.8 Mg ha^{-1} (SE=3.7 Mg ha^{-1}) based on the field survey and 11.9 Mg ha^{-1} (SE=1.6 Mg ha^{-1}), 12.2 Mg ha^{-1} (SE=1.9 Mg ha^{-1}), and13.7 Mg ha^{-1} (SE=2.1 Mg ha^{-1}) for the model-assisted approaches.

[TABLE 8]

Apart from the deforestation post-stratum, the field-based and model-assisted estimates were fairly consistent. The uncertainties were clearly smaller for the model-assisted approach. The relative efficiency was 2.4-3.3 for deforestation, 13.7-38.7 for degradation, 1.5-2.4 for untouched, and 3.1-5.3 for the overall net change estimate. In a study where model-assisted estimates of standing biomass were obtained with support of LiDAR data, the relative efficiency of the model-assisted estimates compared to a pure field-based estimate was 5.3 (Næsset et al., 2011). Thus, it seems like a similar gain in efficiency can be obtained for change as well, provided that proper models are available. Some differences were observed between the three modeling approaches. Apart from the deforestation post-stratum, the simple linear models providing direct predictions of change (approach A) resulted in better precision than the two other modeling approaches. This is consistent with recent findings by Bollandsås et al. (2012).

The relative performance of the model-assisted estimation of change for the entire population seems to be highly dependent on the magnitude of the different types of changes in the landscape. Especially for degradation the support of LiDAR as auxiliary information was of great value. The models for change in biomass for this particular category also showed very strong relationships, regardless of modeling approach (R^2= 0.88-0.98, Table 6).

It should be mentioned that in the post-stratification the post-strata were not determined independently of the sample since the logistic regression model used to predict post-stratum for the individual population elements was fitted on the sample data. Such post-stratification is known as endogenous post-stratification. This dependency will tend to add variability to the estimators. However, Breidt & Opsomer (2008) concluded that the practical effects were minimal even for relatively small sample sizes.

Nevertheless, some caution should be exercised. The degradation post-stratum contained only 13 sample plots. Because the survey was pre-stratified the sample sizes for some of the pre-stratum×post-stratum groups which were the basic units of the estimation (see e.g. Eqs. 18 and 29), were very small. In fact, for pre-stratum 2 the fraction that was predicted to be degraded had n=2 and similarly n=4 for the deforestation post-stratum. It is recommended to avoid sample sizes smaller than five (Thompson, 2002) or 10 (Särndal et al., 1992). This particular study covered a time span of 11 years. For shorter time periods, say, 1-5 years, which probably would be more relevant for official reporting of changes in biomass and carbon stocks, the challenges of having few samples in change categories representing human activities for which estimates are required would be substantial. A pre-stratification also makes the design less robust than a simple and unstratified design in the sense that a pre-stratification followed by a subsequent post-stratification may result in a large number of distinct groups that have to be handled as unique entities through the estimation procedure.

One way to mitigate the risk of few samples in rare change categories (post-strata) is to increase the sampling intensity in areas where changes are expected to occur, for example along deforestation frontiers, i.e., buffer zones surrounding recently deforested areas where continued land conversion might be expected in the future. However, the geographical location of future loss of biomass can be difficult to predict and much of the loss is also related to daily use of tree biomass in the local communities leading to degradation rather than deforestation or even just temporary loss of trees. Thus, when resources for field sampling are scarce application of design-based estimators for change is challenging since they rely on probability samples of sufficient sizes for each part of a forest for which separate estimates are requested.

This study was focused on how LiDAR data may assist in providing areal estimates of changes typically required for international reporting and how associated change estimates for biomass can be obtained. The study did not address how one most efficiently ("minimizing" the uncertainty) could estimate net change in biomass for the entire AOI, given the available resources, i.e., the field sample and the LiDAR data at hand. For example, it is likely that more efficient post-stratification schemes than the applied one (deforestation/degradation/untouched) may exist. Thus, had the aim of this work been to provide "the most precise" estimate of net change in biomass for the entire AOI regardless of activity, we would have considered other post-stratification schemes as well. This could also incorporate a separate class representing those parts of the population where prediction of post-stratum according to a model would be uncertain (cf. Frayer, 1978; Gregoire & Valentine, 2008, p. 153) and a fine-tuning of the probability thresholds applied when assigning specific categories to each individual population element according to the model.

In general, the focus in international reporting on human activity categories in many cases is sub-optimal in the sense that the uncertainty of the estimated overall net change in carbon is likely to be larger than it needs to be, given the resources spent on data collection. Estimates with higher precision can most likely be achieved within given budgets with more conscious selection of pre-/post-stratification schemes and a careful choice of estimation procedures.

Finally, it should be mentioned that little attention was vested on finding the "best" models for prediction of change category (post-stratum) as well as change in biomass. Other model forms, transformations of the LiDAR variables, and more sophisticated variable selection procedures (McRoberts et al., 2012b) may provide more suitable models and thus provide even more precise model-assisted estimates.

4. Conclusions

To conclude, this study has demonstrated how multi-temporal LiDAR data may be used as auxiliary to data from a probability sample of field plots to estimate areal changes in a forest and associated changes in biomass deemed relevant for international reporting. The change categories were treated as post-strata in the estimation. The empirical results indicate a significant gain in precision of areal estimates of deforestation, forest degradation, and untouched areas by adding LiDAR data to the estimation. Compared to pure field-based estimates, the standard errors of the model-assisted estimates were reduced by 43-75%, with the largest relative improvement for deforestation. The LiDAR data also contributed to improved precision of the biomass change estimates. The standard errors for individual change categories (post-strata) were reduced by 18-84%. The largest improvement in precision was experienced for degradation (73-84%), which is a category that is difficult to assess with most other remote sensing techniques. Small sample sizes can be a challenge in change estimation. Future research should focus on stratification schemes that may contribute to improved precision of change estimates in sample surveys using LiDAR data as auxiliary information with due attention to sample sizes. Other approaches to estimation and inference for which a probability sample of sufficient size is not a prerequisite, such as model-based methods, also deserve attention since resources for field sampling often are scarce in many countries likely to take part in a future REDD mechanism.

Acknowledgments

This research has been funded by the Research Council of Norway (project #184636/S30: “Effects of changing climate on the alpine tree line and mountain forest carbon pools along 1500 km N-S and elevation gradients”). The authors would like to thank Mr. Arild Veidahl, one of the local forest owners who provided us with all necessary facilitates to conduct the field inventories, and Mr. Vegard Lien of the Norwegian University of Life Sciences who provided technical assistance with the GPS work. Blom Geomatics, Norway, is acknowledged for collection and processing of the airborne LiDAR data. We are also grateful to our good colleague Dr. Ron McRoberts of the US Forest Service, St. Paul, Minnesota, and to the two anonymous reviewers for their valuable comments on the manuscript.

References

Andersen, H.-E., Barrett, T., Winterberger, K., Strunk, J., & Temesgen, H. (2009). Estimating forest biomass on the western lowlands of the Kenai Peninsula of Alaska using airborne lidar and field plot data in a model-assisted sampling design. Proceedings of the IUFRO Division 4 conference, Extending forest inventory and monitoring over time and space, 19-22 May 2009, Quebec City, Canada. Available at: http://blue.for.msu.edu/meeting/proceed.php. (last accessed: February 2010).

Andersen, H.-E., & Breidenbach, J. (2007). Statistical properties of mean stand biomass estimators in a LIDAR-bases double sampling forest survey design. Proceedings of the ISPRS Workshop Laser Scanning 2007 and SilviLaser 2007. 12-14 September 2007, Espoo, Finland. IAPRS, Volume XXXVI, Part 3 / W52, 2007, pp. 8-13.

Anon. (2004). SAS/STAT 9.1 User's Guide. SAS Institute Inc., Cary, NC.

Anon. (2005). TerraScan user’s guide. Terrasolid Ltd., Jyvaskyla, Finland, 169 pp. (www.terrasolid.fi) (last date accessed: 2 October 2006).

Anon. (2009). Memorandum of Understanding between the Government of the Cooperative Republic of Guyana and the Government of the Kingdom of Norway regarding Cooperation on Issues related to the Fight against Climate Change, the Protection of Biodiversity and the Enhancement of Sustainable Development [online]. http://www.regjeringen.no/upload/MD/Vedlegg/Klima/klima_skogprosjektet/The%20Memorandum%20of%20Understanding%20Guyana%20Norway%20on%20REDD%20(081109)%20signed%20091109.pdf [accessed 19 September 2011].

Anon. (2010). Final draft: forest carbon partnership facility (FCPF), readiness preparation proposal (R-PP), United Republic of Tanzania [online]. http://www.reddtz.org/ [accessed 10 October 2012].

Asner, G.P., Powell, G.V.N., Mascaro, J., Knapp, D.E., Clark, J.K., Jacobson, J., Kennedy-Bowdoina, T., Balajia, A., Paez-Acostaa, G., Victoriac, E., Secadad, L., Valquid, M., & Hughes, R.H. (2010). High-resolution forest carbon stocks and emissions in the Amazon. Proc., National Academy of Science, 107, 16738-16742.

Axelsson, P. (2000). DEM generation from laser scanner data using adaptive TIN models. Int. Arch. Photogramm. Remote Sens., 33(B4), 110-117.

Blingsmo, K. (1988). Tilvekstfunksjoner. Foredrag fra et seminar angående planlegging i skogbruket (in Norwegian only). Norwegian Forest Research Institute, Ås, 8 pp.

Bollandsås, O.M., Gregoire, T.G., Næsset, E., & Øyen, B.-H. (2012). Detection of biomass change in a Norwegian mountain forest area using small footprint airborne laser scanner data. In submission.

Breidt, F. J., & Opsomer, J. G. (2008). Endogenous post-stratification in surveys: Classifying with a sample-fitted model. The Annals of Statistics, 36, 403-427.

Clark, M.L., Clark, D.B., & Roberts, D.A. (2004). Small-footprint lidar estimation of sub-canopy elevation and tree height in a tropical rain forest landscape. Remote Sens. Environ., 91, 68-89.

Cochran, W.G. (1977). Sampling techniques, 3rd edition. Wiley, New York.

Corona, P., & Fattorini, L. (2008). Area-based lidar-assisted estimation of forest standing volume. Canadian Journal of Forest Research, 38, 2911-2916.

Drake, J.B., Dubayah, R.O., Knox, R.G., Clark, D.B., & Blair, J.G. (2002). Sensitivity of large-footprint lidar to canopy structure and biomass in a neotropical rainforest. Remote Sens. Environ., 81, 378-392.

Drake, J.B, Knox, R.G., Dubayah, R.O., Clark, D.B., Condit, R., Blair, B., & Hofton, M. (2003). Above-ground biomass estimation in closed canopy Neotropical forests using lidar remote sensing: factors affecting the generality of relationships. Global Ecology & Biogeography, 12, 141-159.

Ene, L.T., Næsset, E., Gobakken, T., Gregoire, T.G., Ståhl, G., & Nelson, R. (2012). Assessing the accuracy of regional LiDAR-based biomass estimation using a simulation approach. Remote Sensing of Environment, 123, 579-592.

Frayer, W.E. (1978). Stratification in double sampling – The easy way out may sometimes be the best way. Resource Inventory Notes BLM-10. Denver, Colorado: Bureau of Land Management, U.S. Department of Interior.

Gobakken, T., & Næsset, E. (2008). Assessing effects of laser point density, ground sampling intensity, and field sample plot size on biophysical stand properties derived from airborne laser scanner data. Canadian Journal of Forest Research, 38, 1095-1109.

Gobakken, T., Næsset, E., Nelson, R., Bollandsås, O.M., Gregoire, T.G., Ståhl, G., Holm, S.,Ørka, H.O, & Astrup, R. (2012). Estimating biomass in Hedmark County, Norway using national forest inventory field plots and airborne laser scanning. Remote Sensing of Environment, 123, 443-456.

Goeman, J.J, & Le Cessie, S. (2006). A goodness-of-fit test for multinomial logistic regression. Biometrics, 62, 980-985.

Gregoire, T.G., Ståhl, G., Næsset, E., Gobakken, T., Nelson, R., & Holm, S. (2011). Model-assisted estimation of biomass in a LiDAR sample survey in Hedmark county, Norway. Canadian Journal of Forest Research, 41, 83-95.

Gregoire, T.G., & Valentine, H.T. (2008). Sampling strategies for natural resources and the environment. Chapman & Hall/CRC, Boca Raton, Fla. 474 pp.

Harter, H.L. (1970). Order statistics and their use in testing and estimation. Vol II. US Government Printing Office. Washington D.C. 172 pp.

Holmgren, J. (2004). Prediction of tree height, basal area and stem volume in forest stands using airborne laser scanning. Scand. J. For. Res., 19, 543-553.

Hopkinson, C., Chasmer, L., & Hall, R.J. (2008). The uncertainty in conifer plantation growth prediction from multi-temporal lidar datasets. *Remote Sensing of Environment*, *112*, 1168-1180.

Lefsky, M.A., Cohen, W.B., Harding, D.J., Parker, G.G., Acker, S.A., & Gower, S.T. (2002). Lidar remote sensing of above-ground biomass in three biomes. Global Ecology & Biogeography, 11, 393-399.

Magnussen, S. (1999). Effect of plot size on estimates of top height in Douglas-fir. Western Journal of Applied Forestry, 14, 17-27.

Maltamo, M., Eerikainen, K., Packalén, P., & Hyyppä, J. (2006). Estimation of stem volume using laser scanning-based canopy height metrics. Forestry, 79, 217-229.

Mandallaz, D. (2008). Sampling techniques for forest inventories. Chapman & Hall/CRC, 256 pp.

Marklund, L.G. (1988). Biomass functions for pine, spruce and birch in Sweden. Umeå: Swedish University of Agricultural Sciences, Department of Forest Survey. (In Swedish.)

McRoberts, R.E. (2010). Probability- and model-based approaches to inference for proportion forest using satellite imagery and ancillary data. Remote Sensing of Environment, 114, 1017-1025.

McRoberts, R.E. (2011). Satellite image-based maps: Scientific inference or pretty pictures? Remote Sensing of Environment, 115, 715-724.

McRoberts, R.E., Cohen, W.B., Næsset, E., Stehman, S.V., & Tomppo, E.O. (2010). Using remotely sensed data to construct and assess forest attribute maps and related spatial products. Scandinavian Journal of Forest Research, 25, 368-381.

McRoberts, R.E., Gobakken, T., & Næsset, E. (2012a). Post-stratified estimation of forest area and growing stock volume using lidar-based stratifications. Remote Sensing Environment, 125, 157-166.

McRoberts, R.E., Næsset, E., & Gobakken, T. (2012b). Inference for lidar-assisted estimates of growing stock volume, in submission.

Mukama, K., Mustalahti, I., & Zahabu, E. (2012). Participatory forest carbon assessment and REDD+: Learning from Tanzania. International Journal of Forestry Research, 2012, 14 pp, doi: 10.1155/2012/126454.

Næsset, E. (2002). Predicting forest stand characteristics with airborne scanning laser using a practical two-stage procedure and field data. Remote Sens. Environ., 80, 88-99.

Næsset, E. (2004). Accuracy of forest inventory using airborne laser-scanning: evaluating the first Nordic full-scale operational project. Scand. J. For. Res., 19, 554-557.

Næsset, E. (2007). Airborne laser scanning as a method in operational forest inventory: Status of accuracy assessments accomplished in Scandinavia. Scand. J. For. Res., 22, 433-442.

Næsset, E. (2011). Estimating above-ground biomass in young forests with airborne laser scanning. International Journal of Remote Sensing, 32, 473-501.

Næsset, E., & Bjerknes, K.-O. (2001). Estimating tree heights and number of stems in young forest stands using airborne laser scanner data. Remote Sensing of Environment, 78, 328-340.

Næsset, E., Bollandsås, O.M., & Gobakken, T. (2005). Comparing regression methods in estimation of biophysical properties of forest stands from two different inventories using laser scanner data. Remote Sensing of Environment, 94, 541-553.

Næsset, E., & Gobakken, T. (2005). Estimating forest growth using canopy metrics derived from airborne laser scanner data. Remote Sensing of Environment, 80, 88-99.

Næsset, E., & Gobakken, T. (2008). Estimation of above- and below-ground biomass across regions of the boreal forest zone using airborne laser. Remote Sensing of Environment, 112, 3079-3090.

Næsset, E., Gobakken, T., Solberg, S., Gregoire, T.G., Nelson, R., Ståhl, G., & Weydahl, D. (2011). Model-assisted regional forest biomass estimation using LiDAR and InSAR as auxiliary data: A case study from a boreal forest area. Remote Sensing of Environment, 115, 3599-3614.

Nelson, R. (1997). Modeling forest canopy heights: The effects of canopy shape. Remote Sens. Environ., 60, 327-334.

Nelson, R., Gobakken, T., Næsset, E., Gregoire, T.G., Ståhl, G., Holm, S., & Flewelling, J. (2012). Lidar sampling - Using an airborne profiler to estimate forest biomass in Hedmark County, Norway. Remote Sensing of Environment, 123, 563-578.

Nelson, R., Oderwald, R., & Gregoire, T.G. (1997). Separating the ground and airborne laser sampling phases to estimate tropical forest basal area, volume, and biomass. Remote Sens. Environ., 60, 311-326.

Parker, R.C., & Evans, D.L. (2004). An application of LiDAR in a double-sampling forest inventory. Western Journal of Applied Forestry, 19, 95-101.

Pesonen, A., Maltamo, M., & Kangas, A. (2010). The comparison of airborne laser scanning-based probability layers as auxiliary information for assessing coarse woody debris. Int. J. Remote Sensing, 31, 1245-1259.

Pigeon, J.G, & Heyse, J.F. (1999). An improved goodness-of-fit statistic for probability prediction models. Biometrical Journal, 41, 71-82.

Rypdal, K., Bloch, V.V.H., Flugsrud, K., Gobakken, T., Hoem, B., Tomter, S.M., & Aalde, H. (2005). Emissions and removals of greenhouse gases Emissions and removals of greenhouse gases from land use, land-use change and forestry in Norway. NIJOS report 11/05, Ås, Norway. 105 pp. Ås.

Särndal, C.-E. (1984). Design-consistent versus model-dependent estimation for small domains. Journal of the American Statistical Association, 79, 624-631.

Särndal, C.-E. (2011). Combined inference in survey sampling. Pak. J. Statist., 27, 359-370.

Särndal, C.-E., Swensson, B., & Wretman, J. (1992). Model assisted survey sampling. Springer-Verlag, Inc. New York. 694 pp.

Stehman, S.V. (2009). Model-assisted estimation as a unifying framework for estimating the area of land cover and land-cover change from remote sensing. Remote Sens. Environ., 113, 2455-2462.

Stephens, P.R., Kimberley, M.O., Beets, P.N., Paul, T.S.H., Searls, N., Bell, A., Brack, C., & Broadly, J. (2012). Airborne scanning LiDAR in a double sampling forest carbon inventory. Remote Sens. Environ., 117, 348-357.

St-Onge, B., & Vepakomma, U. (2004). Assessing forest gap dynamics and growth using multi-temporal laser-scanner data. In M. Thies, B. Koch, H. Spiecker, & H. Weinacker (Eds.), Laser-scanners for forest and landscape assessment. Proceedings of the ISPRS working group VIII/2. International Archives of Photogrammetry, Remote Sensing and Spatial Information Sciences, Vol. XXXVI, Part 8/W2. (pp. 173–178).

Thompson, S.K. (2002). Sampling, 2nd ed. John Wiley & Sons, Inc., New York. 367 pp.

Tomppo, E., Gschwantner, T., Lawrence, M., & McRoberts, R.E. (eds.) (2010). National Forest Inventories - Pathways for Common Reporting. Springer, 612 pp.

UNFCCC (2008). Kyoto protocol reference manual on accounting of emissions and assigned amounts. (http://unfccc.int/kyoto_protocol/items/3145.php) (last date accessed: 10 December 2010).

Weishampel, J.F., Blair, J.B., Knox, R.G., Dybayah, R., & Clark, D.B. (2000). Volumetric lidar return patterns from old-growth tropical rainforest canopy. Int. J Remote Sensing, 21, 409-415.

Woodbury, P.B., Smith, J.E., & Heath, L.S. (2007). Carbon sequestration in the U.S. forest sector from 1990 to 2010. For. Ecol. Manage., 241, 14-27.

Yu, X., Hyyppä, J., Kaartinen, H., & Maltamo, M. (2004). Automatic detection of harvested trees and determination of forest growth using airborne laser scanning. Remote Sensing of Environment, 90, 451–462.

Yu, X., Hyyppä, J., Kaartinen, H., Hyyppä, H., Maltamo, M., & Rönnholm, P. (2005). Measuring the growth of individual trees using multi-temporal airborne laser scanning point clouds. In: Proceedings of the ISPRS Workshop Laser Scanning 2005, 12-15 September 2005, Enschede, the Netherlands., 36, pp. 204-208.

Yu, X., Hyyppä, J., Kukko, A., Maltamo, M., & Kaartinen, H. (2006). Change detection techniques for canopy height growth measurements using airborne laser scanner data. Photogrammetric Engineering and Remote Sensing, 72, 1339−1348.

Yu, X., Hyyppä, J., Kaartinen, H., Maltamo, M., & Hyyppä, H (2008). Obtaining plotwise mean height and volume growth in boreal forests using multi-temporal laser surveys and various change detection techniques. International Journal of Remote Sensing, 29, 1367-1386.

Table 1. Areal distribution on forest classes, corresponding sample survey plot numbers, sampling fractions, and estimated total above-ground biomass on the plots in 1999 and 2010.

Forest class	Pre-stratum	Area (ha)	No. of plots	Sampling fraction	AGB_{1999} (Mg ha^{-1})		AGB_{2010} (Mg ha^{-1})	
					Mean	Range	Mean	Range
I: Recently regenerated	1	65.8	31	0.0094	49.2	2.2-171.6	116.6	25.7-220.0
II: Young forest	1	120.9	55	0.0091	114.9	25.6-272.4	172.2	52.2-441.1
III: Mature forest, spruce dominated	1	140.4	58	0.0083	153.8	34.5-349.1	118.7	0-462.3
IV: Mature forest, pine dominated	2	195.6	32	0.0033	94.6	40.8-191.6	95.1	0-195.8

Table 2. Sensor and flight parameters for the airborne scanning LiDAR campaigns

Parameter	1999	2010
Instrument	Optech ALTM 1210	Optech ALTM Gemini
Aircraft	Piper PA-31-310 Navajo	Piper PA-31-310 Navajo
Date of acquisition	8-9 June 1999[a]	2 July 2010
Average flying altitude	700 m a.g.l.	900 m a.g.l.
Flight speed	71 ms^{-1}	80 ms^{-1}
Pulse repetition frequency	10 kHz	100 kHz
Scan frequency	21 Hz	55 Hz
Scan angle (after processing)	14.0°	13.8°
Pulse density on ground	1.2 m^{-2}	7.3 m^{-2}

[a]LiDAR data for terrain modeling acquired on 6 June 2000.

Table 3. Classification rules used to determine the post-stratum for the sample survey plots

Post-stratum	Forest class	Rule
A. Deforestation	I-IV	if $AGB_{2010} < 0.1AGB_{1999}$ then category='A'
B. Degradation	I	elseif $AGB_{2010} \geq 0.1AGB_{1999}$ and $AGB_{2010} < AGB_{1999}$ then category='B'
	II	elseif $AGB_{2010} \geq 0.1AGB_{1999}$ and $N_{2010} < 0.5N_{1999}$ then category='B'
	III-IV	elseif $AGB_{2010} \geq 0.1AGB_{1999}$ and $N_{2010} < 0.7N_{1999}$ then category='B'
C. Untouched	I-IV	elseif category='C'

N_{1999}=observed stem number in 1999, N_{2010}=observed stem number in 2010, AGB_{1999}=observed total above-ground biomass in 1999, AGB_{2010}=observed total above-ground biomass in 2010.

Table 4. Estimation results for multinomial logistic regression model shown in Eq. (1)

Coefficient[a]	Estimate	Wald chi-square	*p*-value
Intercept_B	4.89	2.82	0.093
Intercept_C	7.60	6.79	0.009
$\delta pf70_B$	0.48	5.56	0.018
$\delta pf70_C$	0.83	8.90	0.003
$\delta df0_B$	7.00	2.17	0.141
$\delta df0_C$	36.46	18.52	<0.001
Model fit:			
Deviance			1.000
Pearson chi-square goodness-of-fit			1.000

[a]Subscripts B and C symbolize coefficients in models for post-strata B and C, respectively; $\delta pf70$=difference between 70th height percentiles of the first echo LiDAR data from 2010 and 1999; $\delta df0$=difference between the cumulative canopy densities at 1.3 m above ground of the first echo LiDAR data from 2010 and 1999.

Table 5. Results of leave-one-out cross validation of the multinomial logistic regression model in Table 4. The table shows an error matrix of observed versus predicted number of field plots that were classified into post-strata

	Observed				
Predicted	A	B	C	Totals	User's accuracy (%)
A. Deforestation	22	1	0	23	95.7
B. Degradation	1	9	3	13	69.2
C. Untouched	0	6	134	140	95.7
Totals	23	16	137	176	
Producer's accuracy (%)	95.7	56.3	97.8		
Overall accuracy (%)			93.8		

Table 6. Regression models for change in above-ground biomass (δAGB), for above-ground biomass in 1999 (AGB_{1999}) and 2010 (AGB_{2010}), and for the ratio between biomass in 2010 and 1999 (AGB_{2010}/AGB_{1999})

Post-stratum	Forest class	Response variable	Model form[a]	Explanatory variables[b]	n	R^2
A	All	δAGB	Linear	$\delta dl5$	23	0.60
B	All	δAGB	Linear	$\delta pf0$, $\delta pf20$, δcvf, $\delta pl0$	13	0.98
C	I	δAGB	Linear	$\delta pf20$	31	0.40
C	II	δAGB	Linear	$\delta meanf$	49	0.44
C	III	δAGB	Linear	$\delta df3$, $\delta pl10$, $\delta pl90$	34	0.60
C	IV	δAGB	Linear	$\delta pf50$, $\delta df8$, $\delta pl60$, $\delta pl80$	26	0.77
A	All	AGB_{1999}	Multiplicative	$pf70$, $dl3$	23	0.72
B	All	AGB_{1999}	Multiplicative	$pf30$	13	0.88
C	I	AGB_{1999}	Multiplicative	$pf10$, $df5$	31	0.88
C	II	AGB_{1999}	Multiplicative	$pf20$, $dl1$	49	0.92
C	III	AGB_{1999}	Multiplicative	$pf80$, $dl7$	34	0.81
C	IV	AGB_{1999}	Multiplicative	$pf90$, $df9$	26	0.72
A	All	AGB_{2010}	Multiplicative	$pf90$, $dl5$	23	0.67
B	All	AGB_{2010}	Multiplicative	$meanl$	13	0.93
C	I	AGB_{2010}	Multiplicative	$meanl$, $dl0$	31	0.88
C	II	AGB_{2010}	Multiplicative	$pl40$, $meanl$	49	0.82
C	III	AGB_{2010}	Multiplicative	$meanl$, $df9$	34	0.80
C	IV	AGB_{2010}	Multiplicative	$pl80$, $dl0$	26	0.76
A	All	AGB_{2010}/AGB_{1999}	Multiplicative	$Rdf7$, $Rdf9$, $Rdl4$, $Rdl8$	23	0.95
B	All	AGB_{2010}/AGB_{1999}	Multiplicative	$Rdf5$, $Rdf9$	13	0.92
C	I	AGB_{2010}/AGB_{1999}	Multiplicative	$Rdf0$, $Rdf9$, $Rpl0$, $Rdl1$	31	0.87
C	II	AGB_{2010}/AGB_{1999}	Multiplicative	$Rpl90$, $Rdl8$	49	0.55
C	III	AGB_{2010}/AGB_{1999}	Multiplicative	$Rpl90$, $Rdl6$	34	0.44
C	IV	AGB_{2010}/AGB_{1999}	Multiplicative	$Rpf50$, $Rpl50$, $Rpl90$	26	0.75

[a]Linear models were estimated according to Eq. (38). Multiplicative models were estimated according to Eq. (39).

[b]Symbols: δ=difference between 2010 and 1999 for given variable; R=ratio between 2010 and 1999 for given variable; p=height percentile of vegetation echoes (0, 10, …, 90); d=cumulative canopy density above vegetation threshold (0, 1, …, 9); cv=coefficient of variation of height of vegetation echoes; $mean$=arithmetic mean of height of vegetation echoes; f=first echo; l=last echo.

Table 7. Estimated area ($\hat{A}^g$) and associated standard error estimates (SE) (ha)

Post-stratum	No. of plots	Synthetic estimate	Direct estimate		Model-assisted estimate	
		$\hat{A}^g$	$\hat{A}^g$	SE	$\hat{A}^g$	SE
A. Deforestation	23	51.8	70.4	14.5	51.8	3.4
B. Degradation	13	46.4	44.6	11.8	53.4	6.7
C. Untouched	140	424.5	407.7	17.4	417.5	5.8

Table 8. Estimated change in above-ground biomass (*AGB*) ($\hat{\lambda}_{g\cdot}$) and associated standard error estimates (SE) (Mg ha^{-1})

Post-stratum	No. of plots	Synthetic estimate	Direct estimate		Model-assisted estimate	
		$\hat{\lambda}_{g\cdot}$	$\hat{\lambda}_{g\cdot}$	SE	$\hat{\lambda}_{g\cdot}$	SE
Approach A: Linear models for change in *AGB*:						
A. Deforestation	23	-161.1	-131.8	8.9	-162.7	5.8
B. Degradation	13	-63.3	-45.9	31.1	-62.8	5.0
C. Untouched	140	41.4	43.1	2.8	41.4	1.8
All categories ($\hat{\lambda}$)	176	12.0	17.8	3.7	11.9	1.6
Approach B: A system of nonlinear models for change in *AGB*:						
A. Deforestation	23	-157.1	-131.8	8.9	-158.0	4.9
B. Degradation	13	-47.7	-45.9	31.1	-49.0	8.2
C. Untouched	140	42.4	43.1	2.8	39.7	2.0
All categories ($\hat{\lambda}$)	176	14.6	17.8	3.7	12.2	1.9
Approach C: Change in *AGB* by difference between predictions for 2010 and 1999:						
A. Deforestation	23	-161.4	-131.8	8.9	-162.3	4.9
B. Degradation	13	-52.4	-45.9	31.1	-52.2	8.4
C. Untouched	140	42.8	43.1	2.8	42.4	2.3
All categories ($\hat{\lambda}$)	176	14.1	17.8	3.7	13.7	2.1

Figure Captions

Fig. 1. Map of the Våler study area (852.6 ha) showing the geographical distribution of the four forest classes (*left*) constituting the target population (gray shaded areas), other areas within the study region (white), and the distribution of the systematic sample plots (black dots). Forest classes I-III constitute pre-stratum 1 while forest class IV is identical to pre-stratum 2. The post-stratification produced by logistic regression model predictions is displayed to the *right*.

Fig. 2. LiDAR echoes (>0.5 m) for plot #33 acquired in 2010. Tree heights recorded on 13 trees in 2010 ranged from 0.5 to 4.0 m. Observed above-ground biomass in 2010 was 7.1 Mg ha^{-1}. Gray dots indicate echoes from trees with their stem inside the plot. Black dots indicate laser echoes from a large tree with the stem located on the plot circumference but correctly recorded to have its stem center outside the circumference. Three echoes are located on the stem itself and indicate the actual position of the stem. Maximum recorded LiDAR height for the taller tree was 22.4 m.

FIGURE 1

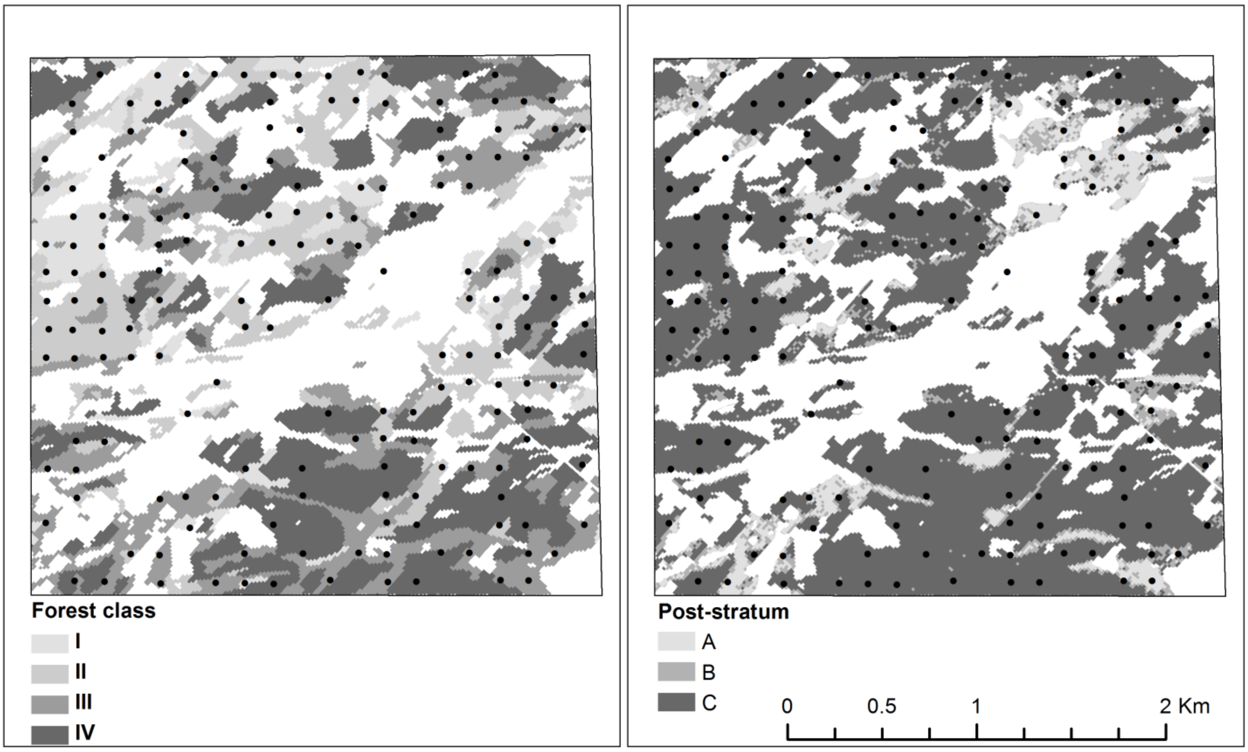

1478 FIGURE 2